INVESTIGATION INTO DENSE NON-AQUEOUS PHASE LIQUID (DNAPL) TRANSPORT AND REMEDIATION IN VERTICAL FRACTURES

by

Kortney A. Adams

B.S. Civil Engineering
Washington University, 1996

Submitted to the Department of Civil and Environmental Engineering in Partial Fulfillment of the Requirements for the Degree of

MASTER OF SCIENCE IN CIVIL AND ENVIRONMENTAL ENGINEERING

at the

MASSACHUSETTS INSTITUTE OF TECHNOLOGY

September, 2000

Signature of Author .....
Department of Civil and Environmental Engineering
August 11, 2000

Certified by .....
Patricia J. Culligan-Hensley
Associate Professor of Civil and Environmental Engineering
Thesis Supervisor

Accepted by .....
Daniele Veneziano
Chairman, Departmental Committee on Graduate Studies

Investigation into Dense Non-Aqueous Phase Liquid (DNAPL) Transport and Remediation in Vertical Fractures

by

Kortney A. Adams

Submitted to the Department of Civil and Environmental Engineering on August 11, 2000, in Partial Fulfillment of the Requirements for the Degree of Master of Science in Civil and Environmental Engineering

Abstract

This thesis investigates the transport behavior of a common category of industrial pollutants, known as Dense, Non-Aqueous Phase Liquids (DNAPLs). These organic chemicals are more dense than water and relatively insoluble. A typical release of DNAPL at the ground surface will migrate downward, relatively unhindered, until it reaches an impermeable clay layer or bedrock, where a pool begins to form. If the clay or bedrock is fractured, DNAPL can invade the fracture system and continue to migrate. Once present in a fracture network, DNAPL can act as an ongoing contaminant source to groundwater, often rendering drinking water supplies unusable. The work described in this thesis is part of a larger project designed to ultimately predict DNAPL behavior in real, rough-walled fracture systems, toward the aim of developing better schemes to locate and remediate it.

The work presented in this thesis examined the invasion behavior of DNAPL in water-saturated, smooth-walled, planar-shaped, vertical fractures. Experiments were performed at a reduced scale using a geotechnical centrifuge. Experimental results demonstrated that a simple static model can reasonably predict the DNAPL pool height that can be developed before fracture invasion occurs. In addition, a dynamic model derived from the Navier-Stokes equations was also shown to reasonably predict the asymptotic displacement behavior of the invading DNAPL, and its behavior at the fracture exit.

This thesis also examined the behavior of DNAPL plugs in water-saturated, smooth-walled, circular-shaped, vertical fractures under upward displacement conditions. These experiments were performed at full-scale in the laboratory. The results demonstrated that a theoretical model based on a pressure balance reasonably predicts the pressure gradient that must be created in the system to mobilize a DNAPL plug trapped in the fracture. Experiments also confirmed that there was no observable water channeling along or through the DNAPL in the smooth-walled fracture, and that the DNAPL displaced as a plug.

The results obtained in these experiments suggest that hydraulic flushing might be developed into a feasible remediation technique for removing residual DNAPL from fractured rock or clay, if the fracture roughness does not significantly alter the flow dynamics.

Thesis Supervisor: Patricia J. Culligan-Hensley

Title: Associate Professor of Civil and Environmental Engineering

Acknowledgements

I wish to express my deepest thanks to the following people who offered their assistance to me during my time at MIT:

- To Professor Patricia J. Culligan-Hensley, for her guidance, support, and never-ending patience throughout the research process, and also for her considerable contributions to this thesis. I was privileged to have her as my advisor.
- To Dr. John T. Germaine, for offering expert laboratory guidance at critical times. Without his suggestions, my research would never have been finished.
- To Mr. Stephen Rudolf, for his cheerful assistance and patience, particularly when I came asking for equipment I couldn't describe.
- To Mr. Laurent Levy and Dr. Kurt Sjoblom, for answering every question I ever threw at them about conducting research or writing a thesis. Thanks especially to Mr. Levy, whose painstaking work with theoretical and centrifuge modeling of DNAPL in fractures laid the foundation upon which this thesis is based.
- To the MIT Geotechnical Group, for making MIT a friendly and fun place to work.
- To my family, roommates, and friends, for their unflagging support. Special thanks to Mr. Fernando Padilla, who helped conduct late-night experiments on more than one occasion.

Thanks to you all for your generosity and kindness.

Table of Contents

Table of Tables

Table of Figures

Chapter 1: Introduction

1.1 Background

During the past several years, the United States Environmental Protection Agency has recognized that groundwater contamination is an increasingly important environmental concern in many industrialized areas [National Research Council 1994]. Of particular concern is a category of organic chemicals that are more dense than water and are immiscible, or virtually immiscible, in water, known as Dense, Non-Aqueous Phase Liquids (DNAPLs). Most DNAPLs are industrial byproducts, such as halogenated solvents, polychlorinated biphenyls (PCBs), pesticides, and coal tars. These chemicals are generated and used in a variety of industries, frequently in large amounts. The most common DNAPLs, such as 1,2-Dichloroethane, 1,1,1-Trichloroethane, and Trichloroethene, are produced in the U.S. at a rate of several hundreds of millions of kilograms per year [Pankow et al. 1996]. Due to accidental spills, poor storage facilities, and inadequate disposal practices, these chemicals are frequently released into the subsurface environment.

Because DNAPLs are more dense than water and relatively insoluble, a typical release at the ground surface will migrate downward through the vadose zone, as well as any sandy aquifer, until it reaches an impermeable clay layer or bedrock (see Figure 1.1). The DNAPL typically follows a complex path from the surface that is dependent on gravity, groundwater flow, and the heterogeneity of the aquifer. Once the DNAPL reaches the impermeable layer, a pool begins to form. If the clay or bedrock system is fractured, under certain conditions, DNAPL will invade the fractures and continue to migrate. It is common to find DNAPL in a fracture system in several forms: DNAPL pools, residual blobs trapped in pore spaces or fractures, and a dissolved aqueous-phase species.

DNAPL trapped in saturated soil or fractured bedrock can act as a contaminant source to groundwater. Although the solubility of DNAPLs in water is low (on the order of a few milligrams per liter or a few grams per liter, depending on the compound [Lide 1993]), DNAPL solubilities are often larger than regulated drinking water standards by several

orders of magnitude [Pankow et al. 1996]. For this reason, DNAPLs often pose a serious ongoing groundwater contamination problem when present in the subsurface environment.

The difficulties associated with the detection and removal of DNAPLs at hazardous waste sites can significantly complicate the site remediation process, especially for highly heterogeneous subsurface formations, such as fractured clay or bedrock. While it is feasible, although difficult, to control or prevent the further spread of a DNAPL plume in fractured media, it is virtually impossible with existing technologies to effectively clean up an already-contaminated fractured system. This is not only because DNAPLs are very hard to locate and extract from a fracture system, but also because the slow release of the contaminant from a rock or clay matrix severely limits recovery efficiency and can significantly extend remediation time.

Many public water supplies and private homes rely on fractured bedrock aquifers for their drinking water. However, since it is so difficult to remediate DNAPL-contaminated fractured systems, particularly to stringent drinking water standards, any contamination of the aquifer can mean the loss of a valuable water supply. Thus, it is important to develop a better understanding of the mechanisms involved in DNAPL migration in fracture systems, in order to develop better technologies both to locate it and to remediate it.

1.2 Previous Related Work

Initial research into DNAPL migration in fracture systems primarily focused on defining the conditions where DNAPL would invade saturated, rough-walled fractures. Kueper and McWhorter [1991] observed DNAPL behavior in real fracture systems and developed a model that estimated the required entry pressure as a function of capillary pressures in the DNAPL-water system. Thus, they were able to calculate a theoretical maximum height of DNAPL that could pool on top of a fracture before invasion. This model was further validated by Foster et al. [1996] in a series of field tests.

Kueper et al. [1992] also examined the case of DNAPL leakage from a fractured clay or rock impoundment. Here, they calculated the maximum amount of DNAPL that could pool before leakage occurred, and made predictions of the steady-state rate of leakage from the impoundment.

Reitsma and Kueper [1994] detailed the relationship between capillary pressure and saturation in rock fractures, and were able to produce well-defined capillary pressure-saturation curves for real, rough-walled fractures. Later work [Longino and Kueper 1996; 1999] extended this relationship to develop retention curves as a function of the capillary number (a ratio of viscous to capillary forces) and the Bond number (a ratio of buoyant to capillary forces) and to predict the amount of residual DNAPL for some rough-walled fractures before and after hydraulic flushing.

There has been some experimental success with arresting downward DNAPL migration in real fractures by applying upward hydraulic gradients [Chown et al. 1997], which included the addition of surfactants in the flushing stream to reduce the interfacial tension between DNAPL and water [Longino and Kueper 1995]. Figure 1.2 demonstrates how an upward gradient could be created across a fractured aquitard in order to induce upward DNAPL flow.

Stephens et al. [1998] considered a condition where a perched, fractured clay or rock layer was located between two unconfined sand layers. In this case, DNAPL was not observed to pool above the fracture because of the unsaturated nature of the fracture and underlying aquifer.

Some research has also considered the miscibility of DNAPL, and theorized about its dissolution in saturated fractures and subsequent diffusion into the surrounding rock or clay matrix [Parker et al. 1997; Slough et al. 1999].

Levy et al. [1998] began to examine immiscible DNAPL flow in a vertical fracture under idealized conditions. Modeling the fracture as a circular, vertical capillary tube, these researchers verified Kueper's model for entry pressures and also developed a prediction for the dynamic flow behavior of DNAPL in a circular fracture following invasion. Levy

et al. also confirmed that physical modeling of this problem was possible using a geotechnical centrifuge.

The Kueper and Levy models are further discussed in Section 2.1.

1.3 Objectives of Research

The work described in this thesis is part of a larger project designed to ultimately predict the behavior of DNAPL in real, rough-walled fracture systems. The overall aim of this project is to describe both DNAPL invasion and upward flow (remediation) conditions in a vertical fracture system.

Specifically, the objectives of the work presented here are to verify the applicability of Keuper's model to rectangular capillary tubes (a somewhat better approximation of real fractures than circular tubes), to extend Levy's dynamic flow model to rectangular tubes, and to make some initial observations of DNAPL flow behavior under idealized upward displacement conditions. The scope of this work includes theoretical modeling, laboratory experiments, and physical modeling using the geotechnical centrifuge.

1.4 Outline of Thesis

Chapter 2 of this thesis is a review of the static and dynamic invasion behavior expected for an idealized fracture in the laboratory and in a reduced-scale physical model. The experiments designed to test these models are detailed in Chapter 3. Chapter 4 describes the experimental results obtained by using the geotechnical centrifuge to test a series of physical models, and compares these results to those predicted by the theoretical models. Chapter 5 describes the results obtained from observing a full-scale laboratory model under upward displacement conditions. Finally, Chapter 6 discusses the limits of the experimental process and provides some recommendations for future research.

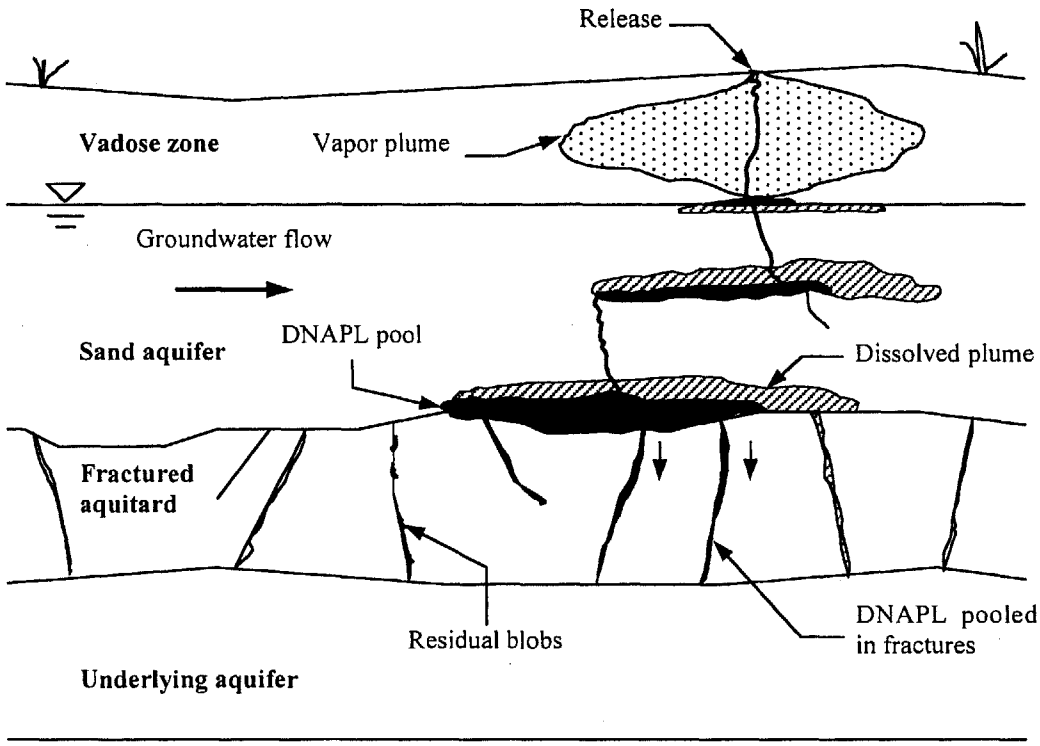

Figure 1.1 Typical scenario of DNAPL release, transport, and accumulation in the subsurface [after Levy et al. 1998].

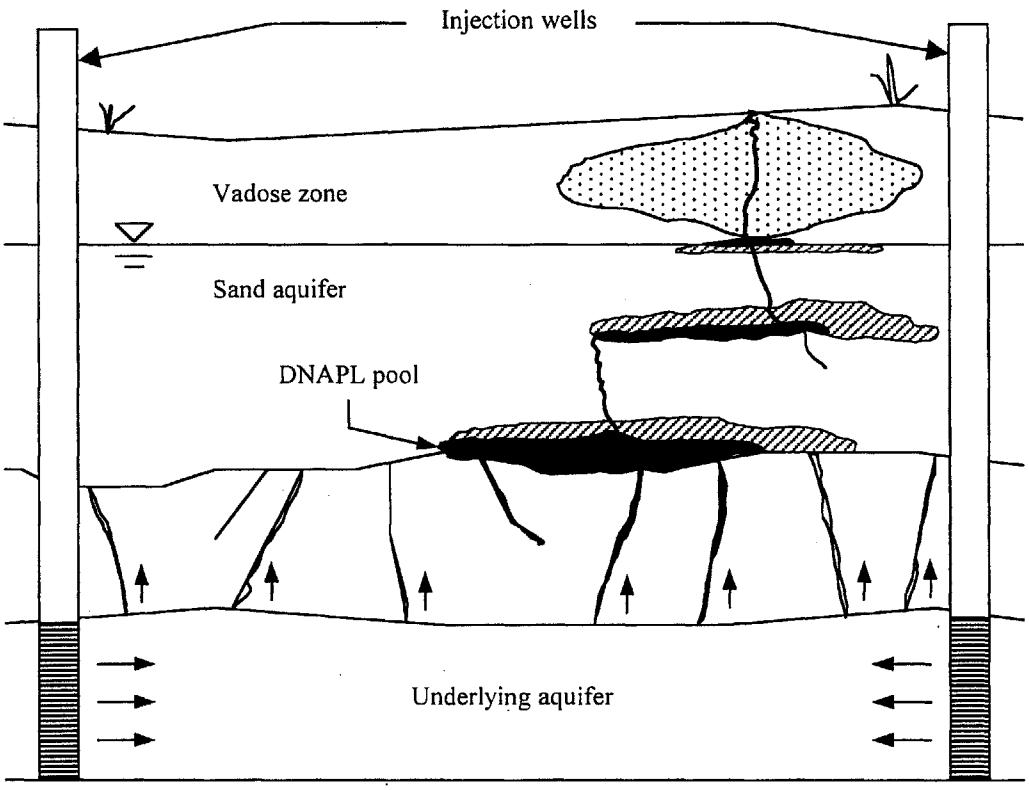

Figure 1.2 Typical method for creation of an upward hydraulic gradient in the field.

Chapter 2: Theory

2.1 Two-Phase Fluid Displacement in Fractures

2.1.1 Static Entry Pressure

In a typical DNAPL contamination scenario, DNAPL pools on a saturated, primarily vertical fracture system. This situation can be idealized by modeling a single fracture as a vertical, circular, capillary tube of diameter d. A DNAPL pool of height h can be simulated using a reservoir tube mounted on top of the capillary tube (see Figure 2.1(a)). Alternatively, the idealized fracture could have a planar shape. In this case, a rectangular capillary tube of aperture d and width a could be used, where a is sufficiently larger than d, so that the tube (or idealized fracture) can be considered infinitely wide (Figure 2.1(b)). In both cases, the capillary tube and attached reservoir are submerged in water.

At the interface of the two liquids in the system, there is a pressure discontinuity due to the interfacial tension between the water and the DNAPL phases. This discontinuity causes a curvature of the interface. The angle between the liquid interface and the wall of the fracture at the point of contact between the interface and the wall is the contact angle, θ. For a DNAPL-water system in fractured clay or rock, water preferentially wets the fracture wall [Bear 1972] and is known as the wetting fluid. The DNAPL is known as the non-wetting fluid. By definition, θ will be less than 90 degrees when measured through the wetting phase.

Pooled DNAPL will invade a fracture if the pressure discontinuity at the interface exceeds the entry pressure of the fracture. In our idealized system, if the diameter of the reservoir tube is sufficiently larger than the diameter of the capillary tube, so that capillary effects associated with the reservoir tube can be ignored, then invasion will occur if [Kueper and McWhorter 1991]

$$\Delta\rho\, gh \geq \frac{2\varepsilon\,\sigma\cos\theta}{d} \tag{2.1}$$

where $\Delta\rho$ is the density contrast between DNAPL and water, g is the acceleration due to gravity, σ is the interfacial tension at the DNAPL-water interface, and ε is equal to 1 for rectangular capillary tubes and 2 for circular tubes. By rearranging the terms of this expression, it is clear that invasion will occur if the DNAPL pool height, h, exceeds some critical height, h_C, defined as

$$h_C = \frac{2\varepsilon\sigma\cos\theta}{\Delta\rho\, g\, d} \tag{2.2}$$

2.1.2 Invasion Dynamics

In their work with circular capillary tubes, Levy et al. [submitted for publication-a] developed a model to describe the dynamic behavior of DNAPL during invasion. In their model, a vertical capillary tube of length l is fed by a DNAPL pool of height $h > h_C$. At time t, the DNAPL has invaded to a depth $x(t)$, where x is the distance from the top of the capillary tube to the tip of the DNAPL-water interface (Figure 2.2). If the diameter of the reservoir tube is sufficiently large compared to the diameter of the capillary tube, then the pool height, h, can be assumed constant during the invasion process. It is also assumed that the longitudinal velocity profile is parabolic and that the radial velocity in each fluid is zero, which is approximately true if the length of the tube, l, is significantly larger than the radius of the tube, r_0 ($r_0 = d/2$).

Assuming that the displacement and velocity of the DNAPL-water interface are zero at $t = 0$, and that the density and viscosity contrasts between DNAPL and water are small compared to the density and viscosity of water, the displacement, x, at time t is

$$x = \Delta h\left[-1 + \frac{1}{2\sqrt{1+\alpha}}\left[\left(-1+\sqrt{1+\alpha}\right)\exp\left(-\frac{g}{2k_w}\left(1+\sqrt{1+\alpha}\right)t\right) + \left(1+\sqrt{1+\alpha}\right)\exp\left(\frac{g}{2k_w}\left(-1+\sqrt{1+\alpha}\right)t\right)\right]\right] \tag{2.3}$$

where

$$\Delta h = h - h_C \tag{2.4}$$

$$k_w = \frac{\rho_w g d^2}{\delta \mu_w} \tag{2.5}$$

$$k_\Delta = \frac{\Delta \rho g d^2}{\delta \mu_w} \tag{2.6}$$

$$\alpha = 4 \frac{k_\Delta k_w}{g l} = \frac{4}{\delta^2} \frac{\Delta \rho \, \rho_w g \, d^4}{\mu_w^2 l} \tag{2.7}$$

ρ_w and μ_w are the density and viscosity of water, δ is equal to 32, k_w is the hydraulic conductivity of water in a capillary tube of diameter d, and k_Δ is the equivalent conductivity of a fluid having the viscosity of water and a density equal to $\Delta\rho$. The dimensionless parameter α describes the magnitude of the inertial forces associated with the system. Large inertial forces correspond to large values of α. For small values of α ($\alpha << 1$), Equation (2.3) simplifies to

$$x = \Delta h \left[-1 + \exp\left(\frac{k_\Delta t}{l} \right) \right] \tag{2.8}$$

Hence, the corresponding velocity at any point in the tube is given by

$$\frac{\mathrm{d}x}{\mathrm{d}t} = k_\Delta \frac{x + \Delta h}{l} \tag{2.9}$$

If invasion takes place as soon as the critical height is exceeded, then Δh is expected to be very small. For x and l significantly larger than Δh, Equation (2.9) reduces to

$$\frac{\mathrm{d}x}{\mathrm{d}t} = k_\Delta \frac{x}{l} \tag{2.10}$$

Equation (2.10) predicts that, as the interface advances in the capillary tube (i.e., as x approaches l and is increasingly larger than Δh), the velocity of the interface is dependent on its position relative to the end of the tube, x/l, not on its absolute position in the tube, x. In addition, the exit velocity at $x = l$ is independent of the length of the tube or

magnitude of interfacial tension forces (expressed in Δh), and is, instead, equal to k_Δ. This model is useful because, in practice, it is very difficult to obtain accurate measurements of Δh; however, it is possible to more accurately measure asymptotic behavior. See Levy et al. [submitted for publication-a] for a complete derivation of the dynamic model, including its limitations.

Equations (2.3) to (2.10) can also be proved valid for rectangular capillary tubes. In this case, δ is equal to 12 in Equations (2.5) to (2.7).

2.1.3 Upward Hydraulic Flushing Pressure

To develop a model for the pressure required to mobilize a DNAPL plug in a saturated fracture, the fracture is again idealized as a circular capillary tube of diameter d and length l (fracture B in Figure 2.3). For ease of measuring pressure changes in the system, it is assumed that there is a connected fracture in the network that is filled only with water (fracture A in Figure 2.3). At time $t = 0$, DNAPL has invaded fracture B to a depth h (i.e., h is the height of the DNAPL plug). In this case, both capillary and gravity forces resist upward motion of the plug, which can be induced by an applied upward pressure.

Capillary forces result from the difference in pressure between the NAPL phase and the water phase at the DNAPL-water interface. The interface is stationary at equilibrium; for circular tubes, this condition can be expressed as

$$\left(P_N - P_W\right)\frac{\pi}{4}d^2 = \sigma\cos\theta(\pi d) \tag{2.11}$$

where P_N is the pressure in the NAPL phase, P_W is the pressure in the water phase, and σ and θ are as defined above. By rearranging terms, the capillary force can be expressed as

$$P_C = P_N - P_W = \frac{4\sigma\cos\theta}{d} \tag{2.12}$$

Gravity forces are due to the density difference between DNAPL and water. The gravity force resulting from replacing a given volume of water with an equivalent volume of DNAPL can be expressed as

$$P_G = \frac{\frac{\pi}{4} d^2 (\rho_N g - \rho_W g) h}{\frac{\pi}{4} d^2} = \Delta \rho g h \tag{2.13}$$

where ρ_N is the density of the DNAPL, ρ_W is the density of water, and $\Delta\rho$ is the difference between the two.

If the pressure in the system is increased, the water level in fracture A will increase proportionally. If the water level in fracture B remains constant, and the radius of fracture A is sufficiently large so that capillary effects are negligible, then the pressure applied to the system can be measured as

$$P_{appl} = \rho_W g (z_A - z_B) = \rho_W g \Delta z \tag{2.14}$$

where z_A is the elevation of the water surface in fracture A, z_B is the elevation of the water surface in fracture B, and Δz is the difference between the two. This relationship is identical to that used to make pressure measurements in a standard u-tube manometer.

If it is assumed that the DNAPL will displace as a plug, so that there will be no water channeling along the edges of the tube, then the plug will be expected to mobilize when the applied pressure exceeds the capillary and gravity forces. This condition can be expressed as

$$P_{appl} \geq P_G + P_C \tag{2.15}$$

or

$$\rho_w g \Delta z \geq \Delta \rho g h + \frac{4 \sigma \cos \theta}{d} \tag{2.16}$$

Rearranging terms to isolate Δz yields a critical applied pressure head, Δz_C, which is defined as

$$\Delta z_C = \frac{\Delta \rho}{\rho_w} h + \frac{4\sigma \cos\theta}{\rho_w g d} \tag{2.17}$$

Hence, the DNAPL plug will mobilize if Δz exceeds the critical value, Δz_C.

2.2 Geotechnical Centrifuge Modeling

2.2.1 Centrifuge Scaling Laws

To avoid the difficulties and expense associated with full-scale field tests, and also to enable the performance of repeatable tests in a controlled laboratory environment, invasion experiments were performed using small-scale models in a geotechnical centrifuge.

It has been demonstrated that the mechanical behavior of a prototype under the earth's gravity, g, can be replicated in a geotechnical centrifuge using a small-scale $1/n$ model of the prototype subjected to a centrifugal acceleration ng (Figure 2.4). As long as the product of depth times gravitational acceleration is the same at all corresponding points in the model and prototype, the stress and fluid pressure distributions throughout the model and prototype will be identical.

To develop equations for a prototype n-times larger than a centrifuged model, the following prototype variables must be defined:

$$X = n\,x \tag{2.18}$$

$$H = n\,h \tag{2.19}$$

$$\Delta H = n\,\Delta h \tag{2.20}$$

$$L = n\,l \tag{2.21}$$

$$T = n^2\,t \tag{2.22}$$

The convention that lowercase variables represent parameters in the centrifuge model and uppercase variables represent the corresponding parameters in the prototype has been adopted. Equations (2.18) to (2.22) are established centrifuge scaling relationships for flow phenomena in geologic media [Culligan-Hensley and Savvidou 1995]. All macroscopic lengths have been scaled by a factor of n. The capillary tube diameter, d, has not been scaled by a factor of n. This is because microscopic lengths, such as soil grain sizes and fracture apertures, must be equivalent in the prototype and centrifuge model in order to correctly scale the system and accurately replicate NAPL behavior in the subsurface [Culligan and Barry 1998]. Transport times have been scaled by a factor of n^2, to accurately model prototype behavior. If the idealized fracture shown in Figure 2.2 were subjected to a centrifugal acceleration equivalent to n-times the earth's gravitational acceleration, the system would model an equivalent prototype given by Figure 2.5.

2.2.2 Centrifuge Modeling of DNAPL Invasion

When the idealized fracture system is placed in the centrifuge and subjected to a centrifugal acceleration ng, the critical height predicted by Equation (2.2) becomes

$$h_c = \frac{2\varepsilon\sigma\cos\theta}{\Delta\rho(ng)d} \tag{2.23}$$

The parameter α, which is the ratio of inertial forces to viscous forces in the system, is now given by

$$\alpha = \frac{4}{\delta^2}\frac{\Delta\rho\,\rho_w(ng)\,d^4}{\mu_w^2 l} \tag{2.24}$$

Note, α will be a factor of n^2 larger for an experiment on a tube of length l at n times the earth's gravity, ng, than it would be for an experiment on a tube of length $L = nl$ at earth's gravity, g. Therefore, the two experiments are not strictly equivalent and inertial forces can become significant in the centrifuge model even if they are not significant in the

corresponding prototype. However, as long as α is still significantly less than 1, inertial forces may still be neglected, and Equation (2.9) can be written for the prototype as

$$\frac{dX}{dT} = K_{\Delta} \frac{X + \Delta H}{L} \tag{2.25}$$

where

$$K_{\Delta} = \frac{\Delta \rho g d^2}{\delta \mu_w} \tag{2.26}$$

and X, ΔH, L, and T are the prototype variables related to the model variables x, Δh, l, and t, respectively, as defined in Section 2.2.1.

If a prototype critical height, H_C, is also defined where

$$H_C = n\, h_C \tag{2.27}$$

then Equation (2.23) becomes

$$H_C = \frac{2\varepsilon\sigma \cos\theta}{\Delta\rho\, g\, d} \tag{2.28}$$

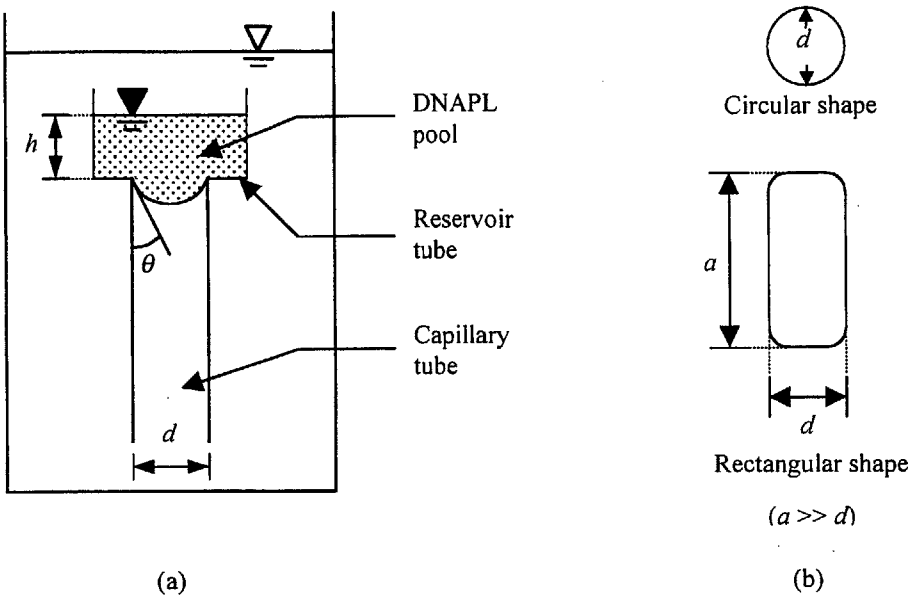

Figure 2.1 (a) Schematic of idealized fracture. (b) Capillary tube cross-sections.

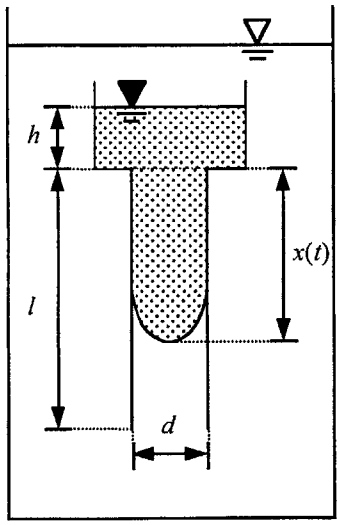

Figure 2.2 Schematic of fracture after invasion begins.

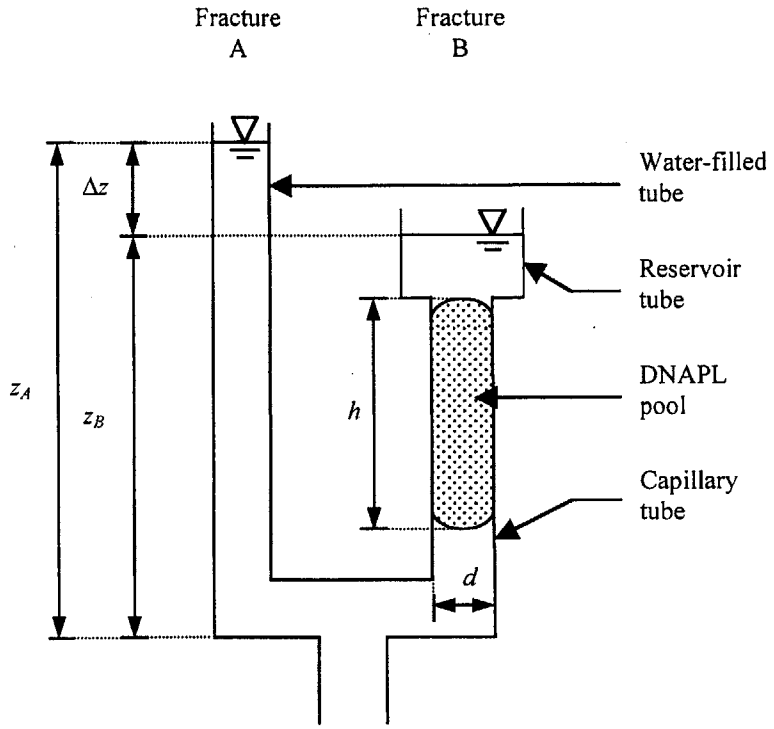

Figure 2.3 Schematic of idealized hydraulic flushing system. Fracture A contains water only. Fracture B has been invaded by DNAPL.

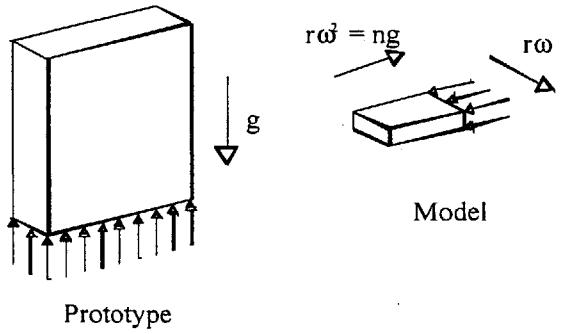

Figure 2.4 Principle of centrifuge modeling [after Schofield 1980].

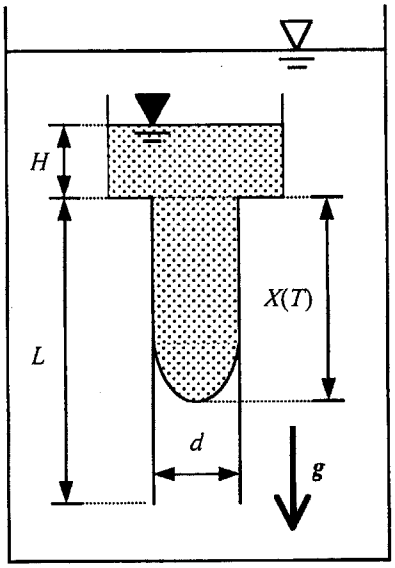

Figure 2.5 Schematic of DNAPL invasion in an equivalent prototype n-times larger than Figure 2.2. X, H, and L are defined in Equations (2.18), (2.19), and (2.21), respectively.

Chapter 3: Experimental Materials and Test Equipment

3.1 Experimental Materials

3.1.1 4-Chlorotoluene

The DNAPL used in all experiments was 4-Chlorotoluene (4-CT). This chemical was selected because of its low density contrast with water, low toxicity, and high flash point (49°C/121°F). In addition, this is the same chemical that was used by Levy et al. [submitted for publication-b] in their experiments, so direct comparisons could be made between their results for invasion in circular tubes and the results obtained here for rectangular tubes.

The relevant properties of 4-CT are provided in Table 3.1. Although the solubility is not zero, it is sufficiently low to consider the DNAPL immiscible in water. In addition, the density and viscosity of 4-CT are close to those of water, which is consistent with the assumptions made in Section 2.1.2. The interfacial tension of 4-CT was not obtainable from literature, so the value listed in Table 3.1 is actually the product $\sigma \cos \theta$, which was measured by Levy et al. [submitted for publication-b] using the capillary rise method.

3.1.2 Sudan IV

To enhance visibility of the DNAPL, and permit tracking of the fluid as it traveled through the fracture system, the 4-CT was dyed red using Sudan IV hydrophobic dye (Aldrich Chemicals) at a concentration of 0.2 g/l. Note that the interfacial tension listed above is for the 4-CT in a dyed state.

3.2 The MIT Geotechnical Centrifuge

All centrifuge experiments were conducted using the balanced-arm centrifuge at the Massachusetts Institute of Technology (MIT). The MIT centrifuge is a Genisco Model 1231 G-Accelerator with a radius of approximately 1.2 m (51 in) and a load capacity of 13,600 *g*-kg (30,000 *g*-lb). The machine has a maximum operating speed of 400 RPM

and can accommodate a maximum payload of 90 kg (200 lb). Based on its load capacity, the centrifuge can rotate a maximum 90-kg (200-lb) mass around its central axis at a velocity of approximately 350 RPM, which would create a centrifugal acceleration 150 times that of the earth's gravitational acceleration (i.e., 150 *g*). At its maximum rotational speed, 400 RPM, which corresponds to an acceleration of 200 *g*, it can rotate a mass of up to 68 kg (150 lb).

A detailed description of this machine is included in Ratnam et al. [1996].

In order to permit observation of the platform and its contents from the centrifuge control room, a small video camera is mounted on the platform. The video camera is a Panasonic Industrial Color CCD Micro-Camera, model GP-KS162, suitable for operation in an elevated gravity field.

3.3 Experimental Procedure - DNAPL Invasion

3.3.1 Experiment Layout

Invasion experiments were performed using a series of rectangular, glass, capillary tubes with nominal apertures of 0.2 mm, 0.5 mm, and 0.6 mm. Tests were also attempted with tubes of 0.1-mm aperture, but these tubes proved to be too small to yield reproducible experimental results. The internal width of each tube was at least 10 times the aperture spacing to minimize edge effects. All tubes were 100 mm in length.

All capillary tubes used were labeled and assigned a number to facilitate tracking and data collection.

The upper part of each capillary tube was connected to a glass reservoir tube using silicone sealant. The internal diameter of each reservoir tube was selected to be at least 10 times the aperture of the capillary tube. In practice, the internal diameters of the reservoir tubes were much larger than required by this constraint, due to the external width of the capillary tube itself.

For each experiment, up to four tubes were secured vertically inside a transparent, rectangular, glass-fronted, centrifuge strong box. A diagram of the experimental setup is included as Figure 3.1.

3.3.2 Test Preparation

Before each test, the capillary and reservoir tubes were soaked overnight in a detergent solution, rinsed with distilled water, triple rinsed with acetone, methanol, and distilled water, and then oven-dried at 200°F for at least 1 hour.

The tubes were then secured inside the centrifuge strong box. The box was subsequently filled with de-aired distilled water and allowed to equilibrate overnight to dissolve any air bubbles that might have become trapped in the system during filling.

A fixed amount of DNAPL was added to each tube using a needle and syringe. In each tube, DNAPL was initially placed at the bottom of the reservoir tube and, as the height of the DNAPL pool increased, the tip of the needle was kept in contact with the DNAPL phase to avoid trapping water droplets between the DNAPL pool and the capillary tube. The height of the DNAPL pool, defined as the distance from the top of the capillary tube to the top of the pool in each reservoir tube, was measured using an optical caliper. In cases where the DNAPL partly wetted the reservoir tube's glass surface and the top of the pool was not a flat surface, the DNAPL pool height was estimated as the average height of the pool in the reservoir tube. The pool heights tested ranged from 10 to 50 mm; these were less than the expected critical heights (on the order of 150 to 450 mm for the tubes tested) so that infiltration into the capillary tube would not occur before centrifuge testing. The strong box and its contents were then transported to the centrifuge.

3.3.3 Centrifuge Testing

After the strong box was secured on the centrifuge platform and the centrifuge arm was balanced, the room was secured and the test begun from the adjacent control room. During each test, the *g*-level was steadily increased by increasing the rotational velocity at a rate of approximately 0.1 RPM per second.

As the g-level increased, the prototype height, H (see Equation (2.19)), also increased until it reached the critical value H_C, at which point invasion occurred. Because the rotational acceleration, and hence the rate of increase of H, were limited to a small value, ΔH was also assumed to be small.

The tube invasion and displacement of the DNAPL-water interface were monitored and recorded using the video camera mounted on the centrifuge platform. RPM data were also recorded during the test and used to later calculate the g-level at invasion. Because the DNAPL travel time through the capillary tube was on the order of seconds, the g-level could be assumed constant throughout the invasion process. In addition, because the internal diameter of the reservoir tube was significantly larger than that of the capillary tube, it was assumed that there was negligible change in h, and therefore H, during the invasion process. This assumption is consistent with the assumptions made in Section 2.1.2.

3.4 Experimental Procedure - DNAPL Flushing

3.4.1 Experiment Layout

Flushing experiments were performed using circular, glass, capillary tubes with nominal internal diameters of 1.3 and 2.7 mm and lengths of approximately 1210 mm. The actual internal diameters of the tubes were calculated by measuring the average volume of water that each size tube could store, and were found to be approximately 1.33 mm and 2.70 mm, respectively.

The bottom of each capillary tube was connected via plastic tubing to a constant flowrate pump, which could be precisely controlled using a control box and a variable power supply. The capillary tube setup was also connected to a graduated cylinder, which was open at the top. This cylinder was used to measure pressure changes in the system, similar to the measuring arm of a u-tube manometer.

The upper part of each capillary tube was connected to a glass reservoir tube using silicone sealant. The internal diameter of the reservoir tube was at least 10 times the

aperture of the capillary tube. The reservoir tube had an overflow port so that a constant water level could be maintained in the reservoir.

The entire setup was mounted vertically in the laboratory. A diagram of the experimental setup is provided in Figure 3.2.

3.4.2 Test Preparation

Before each series of tests, the capillary and reservoir tubes were soaked overnight in a detergent solution, rinsed with distilled water, triple rinsed with acetone, methanol, and distilled water, and then oven-dried for at least 1 hour. The setup was then assembled and filled with distilled water.

After the water levels equilibrated in the reservoir and graduated cylinder, an initial reading of the water level in the system was recorded. DNAPL was then added to the capillary tube using a needle and syringe. Because the diameter of the needle exceeded the internal diameter of the capillary tube for the 1.3-mm series, the DNAPL was pooled on top of the capillary tube and then drawn down into it by retracting the pump and withdrawing water from the system. The larger aperture of the 2.7-mm series allowed DNAPL to be placed directly inside the tube. However, the needle could only penetrate approximately 100 mm into the tube. So, for all tests with plug heights larger than this amount, DNAPL was added to the system by placing up to 100 mm inside the tube, then drawing it down in the tube as described above, then repeating these steps until the desired plug height was achieved. The plug heights tested ranged from 80 to 1149 mm.

For some of the tests, the DNAPL plug extended to the top of the capillary tube. For other tests, however, the plug was submerged in the tube, i.e., there was some distance between the top of the DNAPL plug and the top of the capillary tube. Note that the latter setup may better replicate typical field conditions. In all cases, the addition of DNAPL to the capillary tube raised the water level in the graduated cylinder.

3.4.3 Laboratory Testing

For each experiment, water was introduced to the bottom of the tube at a fixed flowrate. Flowrates used were on the order of 0.002 cm^3/s. The water level in the graduated cylinder increased with the addition of water to the system; the level in the cylinder when the DNAPL plug mobilized was recorded. In addition, the upward displacement of the plug was recorded using the video camera described in Section 3.2.

For several tests, the system was not open to the graduated cylinder. In these cases, the plug displacement was simply monitored with time.

Table 3.1 Properties of 4-Chlorotoluene (4-CT)

Specific Gravity[a]	1.070
Measured Interfacial Tension With Water ($\sigma \cos \theta$)[b], N/m	0.032 ± 0.004
Solubility in Water[c], g/l	1.06×10^{-3}
Viscosity[d], Pa.s	0.9×10^{-3}

[a] Value from Budavari [1996]. Specific gravity at 20°C referred to water at 4°C.

[b] Value from Levy et al. [submitted for publication-b].

[c] Value from Howard and Meylan [1997]. Solubility at 20°C.

[d] Value from Yaws [1995]. Viscosity at 20°C.

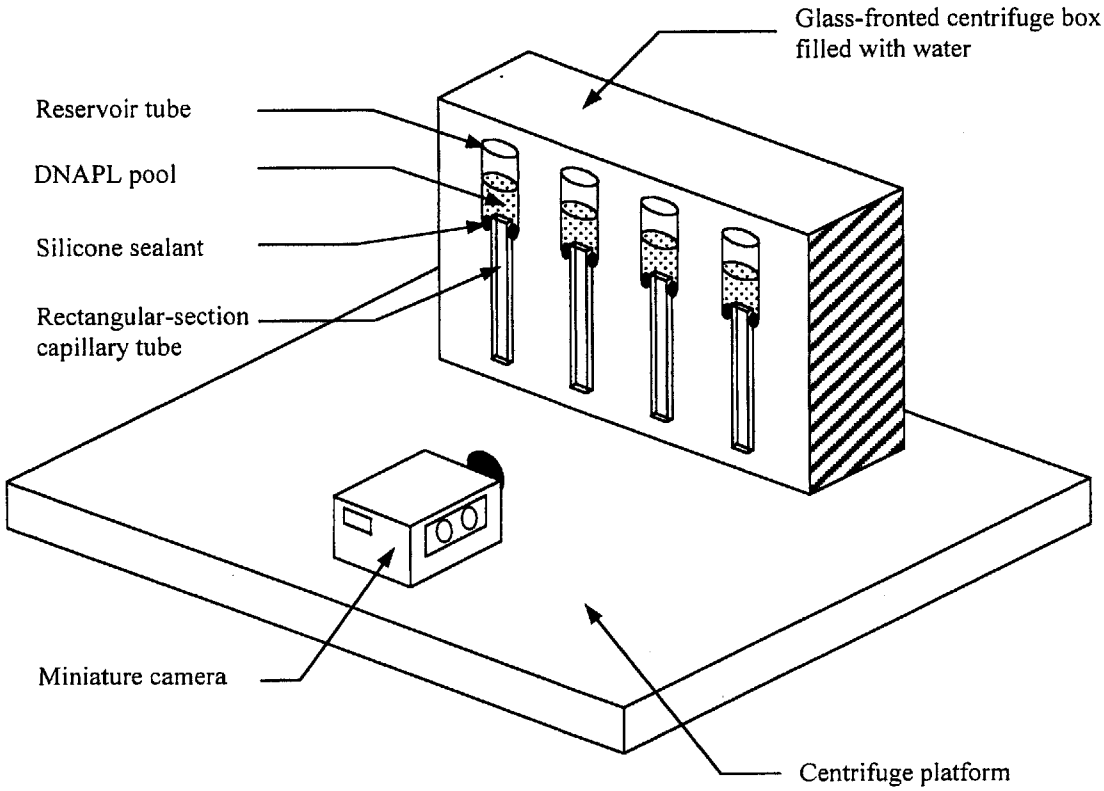

Figure 3.1 Diagram of experimental setup for invasion experiments [after Levy et al. submitted for publication-b].

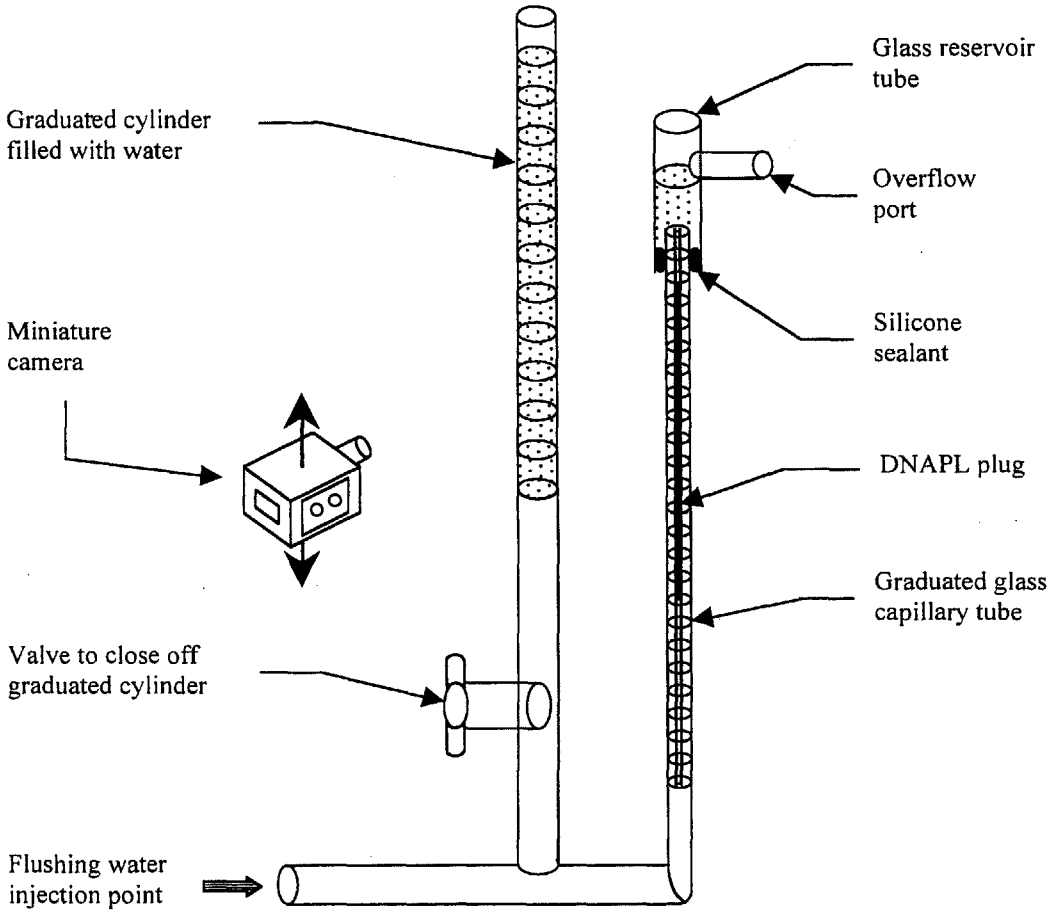

Figure 3.2 Diagram of experimental setup for flushing experiments.

Chapter 4: DNAPL Invasion Test Results and Data

Table 4.1 summarizes the test conditions and results for each centrifuge experiment that was performed. The results are listed in terms of the equivalent prototype data, which were converted from the centrifuge data using Equations (2.18)-(2.22). Levy et al. [submitted for publication-b] demonstrated that these conversions were valid by using the principle of "modeling of models" to verify that centrifuge modeling of DNAPL invasion in circular tubes accurately predicted the DNAPL invasion behavior in corresponding full-scale laboratory experiments.

All tubes tested were 100 mm in length.

4.1 Critical Height Measurements

The measured and predicted values of H_C are compared in Figure 4.1. The predicted values were calculated using Equation (2.28). The width of the prediction zone is due to uncertainty in the value $\sigma \cos \theta$; the upper and lower bounds of the zone are based on the upper and lower limits of the interfacial tension measurement, given in Table 3.1.

Figure 4.1 indicates reasonable agreement between the measured and predicted values. The scatter of data for each aperture size was attributed to the sensitivity of the system to the cleanliness of the tubes, which directly affects the value of $\sigma \cos \theta$. Although the tubes were marked and tracked throughout the experiments, the observed scatter did not correlate with individual tubes.

4.2 Interface Displacement Data

For each test, the displacement of the DNAPL-water interface with time was also recorded. The results obtained for tubes in the 0.2-mm, 0.5-mm, and 0.6-mm series are summarized in Figure 4.2, Figure 4.3, and Figure 4.4, respectively. The data in these figures are again given in terms of prototype conditions.

For comparison, these figures also include theoretical prediction curves, which are the displacement profiles predicted by Equation (2.25) for the given test conditions. With the exception of some of the 0.6-mm tests conducted at higher g levels, values of α were small for the experiments plotted in these figures (see Table 4.1), so Equation (2.25) was applicable. In practice, it was difficult to measure either the time when invasion began or ΔH with reasonable accuracy. It was, however, possible to accurately determine the time when DNAPL exited the tube. Therefore, the exit time was assumed as the point of coincidence between the measured values and the predictions. To generate the theoretical curves, a value of $\Delta H = 0.01\ H_C$ was assumed.

4.3 Data Interpretation

In general, agreement between the measured points and predicted values for both the static and dynamic data are good.

Figure 4.1 indicates reasonable agreement between measured and predicted values of H_C. The prediction appears to be better for smaller aperture tubes. This may be due to the effect of unobservable "pre-infiltration" in larger aperture tubes. In their laboratory work with circular tubes, Levy et al. [submitted for publication-a] observed that, at pool heights significantly less than H_C, a finger of DNAPL would infiltrate the tube a small amount and then displacement would stop. The system would attain equilibrium and no additional displacement would occur without the further addition of DNAPL. This "pre-infiltration" increased the effective pool height, and H_C was taken to be the sum of the pool height and the length of the pre-infiltration finger. The finger was generally longer with increasing tube aperture. It is possible that such pre-infiltration occurred, unobserved, in the centrifuge tests performed here. The true critical heights would therefore be higher than those plotted on Figure 4.1, and therefore in better agreement with the predictions.

The interface displacement data reported in Figure 4.2, Figure 4.3, and Figure 4.4 are in good asymptotic agreement with the model predictions. Equation (2.26) accurately

predicts the exit velocity of the tube, K_{Δ}, which is the slope of the displacement profile at the exit point. Measured values of K_{Δ} are included in Table 4.1 and can be seen to be approximately constant, and independent of the prototype length of the capillary tube.

The value of α increases with g–level and aperture spacing. The agreement between measured and predicted displacement values is subsequently poorer in higher g–level and larger aperture tests as α becomes significant compared to 1, suggesting that inertial forces cannot be neglected (see Figure 4.4).

In all tests, the model overpredicts displacement velocities at early stages of invasion. This was found true no matter what the assumed value of ΔH. Levy et al. [submitted for publication-b] observed the same phenomenon in their work with circular tubes and attributed the discrepancy to the existence of a "capillary region" at the start of the invasion process. Their experiments suggested that, at the early stages of invasion as the DNAPL velocity increases from zero, the dynamic contact angle is less than the value of the static contact angle. This reduced contact angle reduces the value of ΔH, and subsequently the velocity dX/dT. However, as the interface advances in the tube and ΔH becomes negligible compared to X, the model more accurately predicts the measured values.

In their work with circular-section capillary tubes in the laboratory, Levy et al. observed that the length of the capillary region seemed to vary with aperture, but not tube length. For a given aperture size, the length of the capillary region was approximately constant. However, for similar experiments performed in the geotechnical centrifuge, the observed length of the capillary region in the prototype was not a constant, suggesting that DNAPL behavior in the capillary region is not correctly modeled in the centrifuge.

Experimental data for the rectangular-section tubes support this theory. The lengths of the observed capillary regions, at both prototype and model scales, are summarized in Table 4.2, and plotted in Figure 4.5 and Figure 4.6, respectively. Figure 4.5 indicates that

Λ, the length of the capillary region in the prototype, is not constant and increases with increasing g-level. However, in Figure 4.6, λ, the length of the capillary region in the model, is approximately constant, on the order of 70-80 mm. This suggests that the capillary length is primarily a function of the fracture aperture size, not the interface displacement velocity.

It should be emphasized, however, that DNAPL behavior in the capillary region is not believed to be important for real-scale problems. Typical fracture systems have lengths on the order of several meters, and the capillary region should not extend beyond the first few centimeters of a fracture system.

Table 4.1 Summary of Invasion Experiments Performed

Test No.	Tube No.	d (mm)	n	H_c (mm)	α	K_Δ (mm/s)
10	2	0.2	14.6	471	4.6E-03	3.4
	3	0.2	15.8	507	5.0E-03	3.7
12	1	0.2	9.1	419	2.8E-03	2.1
	2	0.2	14.4	508	4.5E-03	3.4
	3	0.2	12.6	508	3.9E-03	3.0
	4	0.2	13.8	425	4.3E-03	3.3
13	2	0.6	11.1	110	0.28	23
	3	0.6	9.2	100	0.23	19
	4	0.6	14.0	138	0.35	30
14	2	0.6	7.0	97	0.18	15
	3	0.6	5.9	90	0.15	13
15	1	0.5	14.4	183	0.18	21
	2	0.5	13.5	179	0.17	20
	3	0.5	12.9	163	0.16	19
	4	0.5	12.0	146	0.15	18
16	1	0.5	9.8	124	0.12	14
	2	0.5	7.0	127	0.09	10
	3	0.5	9.0	153	0.11	13
	4	0.5	10.9	108	0.13	16

Table 4.2 Length of Capillary Region at Prototype and Model Scales

Test No.	Tube No.	d (mm)	n	l (mm)	Capillary Region Prototype Length Λ (mm)	Capillary Region Model Length λ (mm)
10	2	0.2	14.6	100	1170	80
	3	0.2	15.8	100	1270	80
12	1	0.2	9.1	100	820	90
	2	0.2	14.4	100	720	50
	3	0.2	12.6	100	1000	80
	4	0.2	13.8	100	700	51
13	2	0.6	11.1	100	990	89
	3	0.6	9.2	100	640	70
	4	0.6	14.0	100	1400	100
14	2	0.6	7.0	100	490	70
	3	0.6	5.9	100	360	61
15	1	0.5	14.4	100	1020	71
	2	0.5	13.5	100	1120	83
	3	0.5	12.9	100	770	60
	4	0.5	12.0	100	1000	83
16	1	0.5	9.8	100	780	80
	2	0.5	7.0	100	630	90
	3	0.5	9.0	100	630	70
	4	0.5	10.9	100	980	90

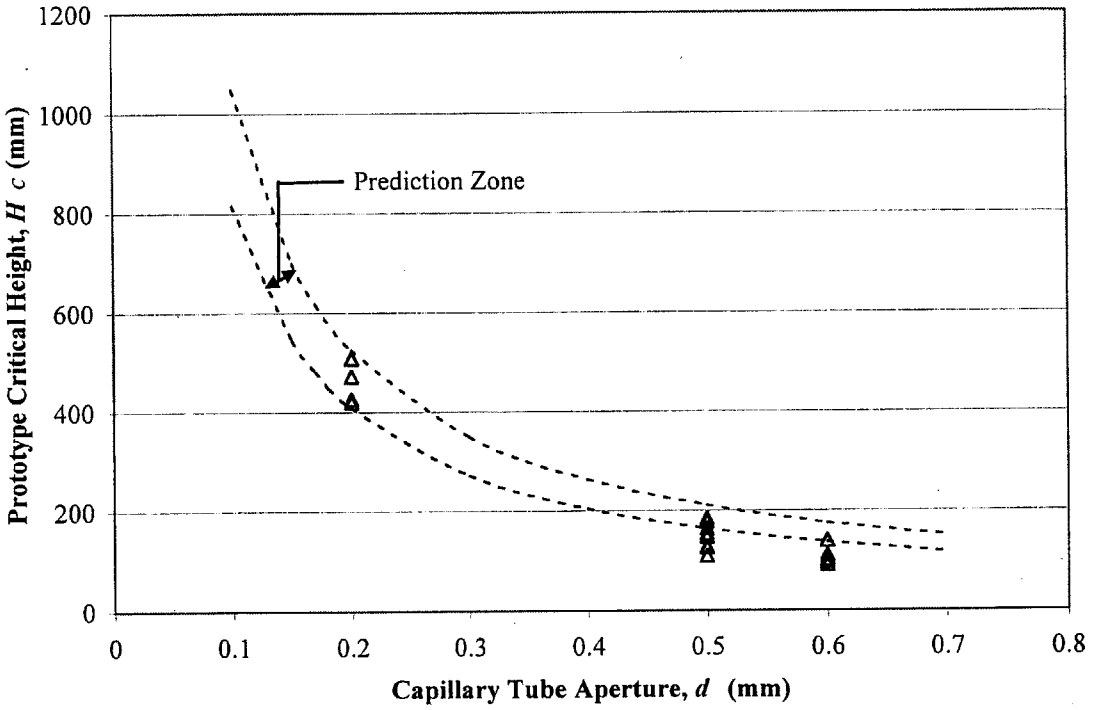

Figure 4.1 Prototype critical heights for capillary tubes of various diameters. Discrete points represent experimental data.

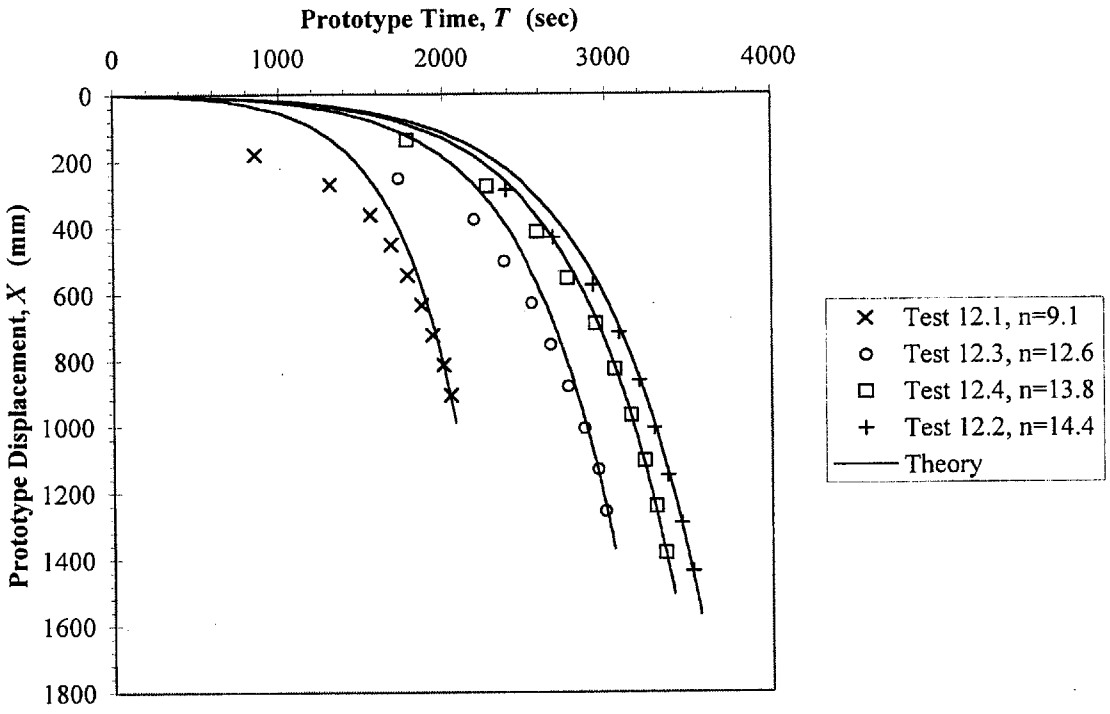

Figure 4.2 Prototype interface displacement versus prototype time for 0.2-mm capillary tube series.

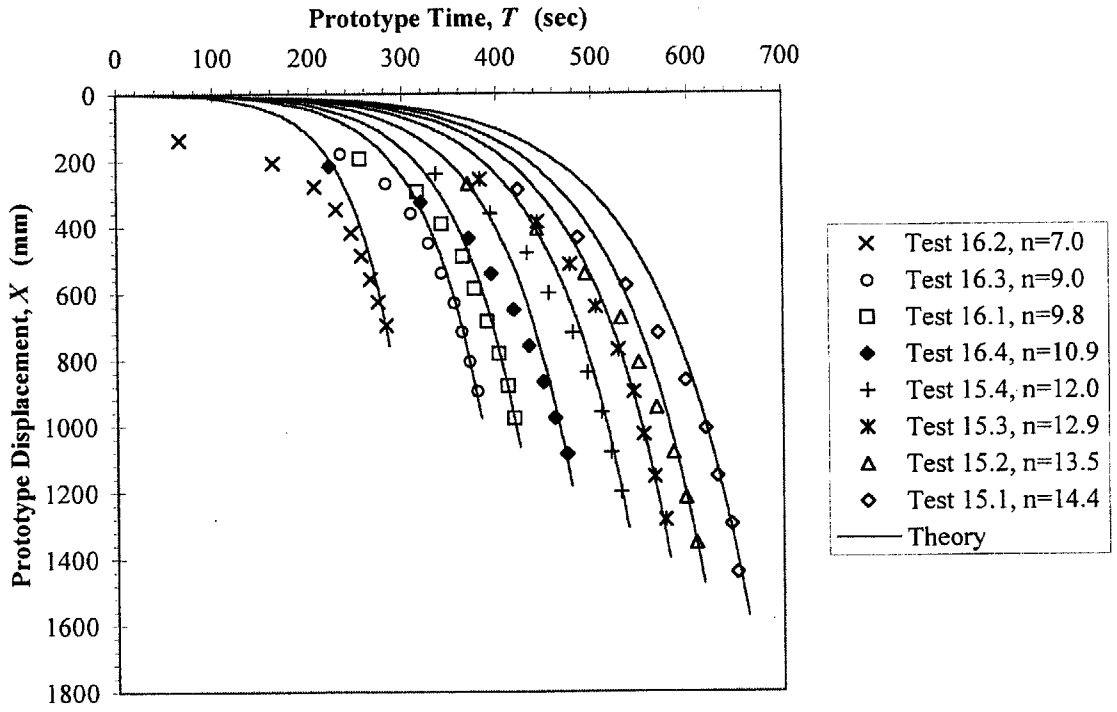

Figure 4.3 Prototype interface displacement versus prototype time for 0.5-mm capillary tube series.

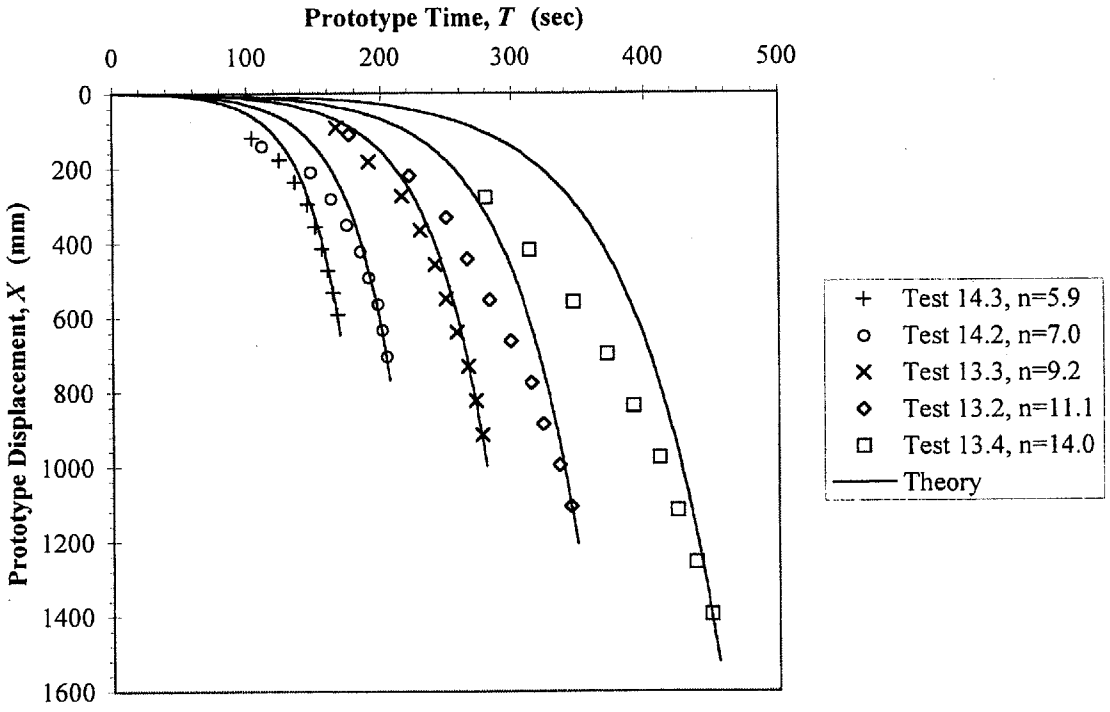

Figure 4.4 Prototype interface displacement versus prototype time for 0.6-mm capillary tube series.

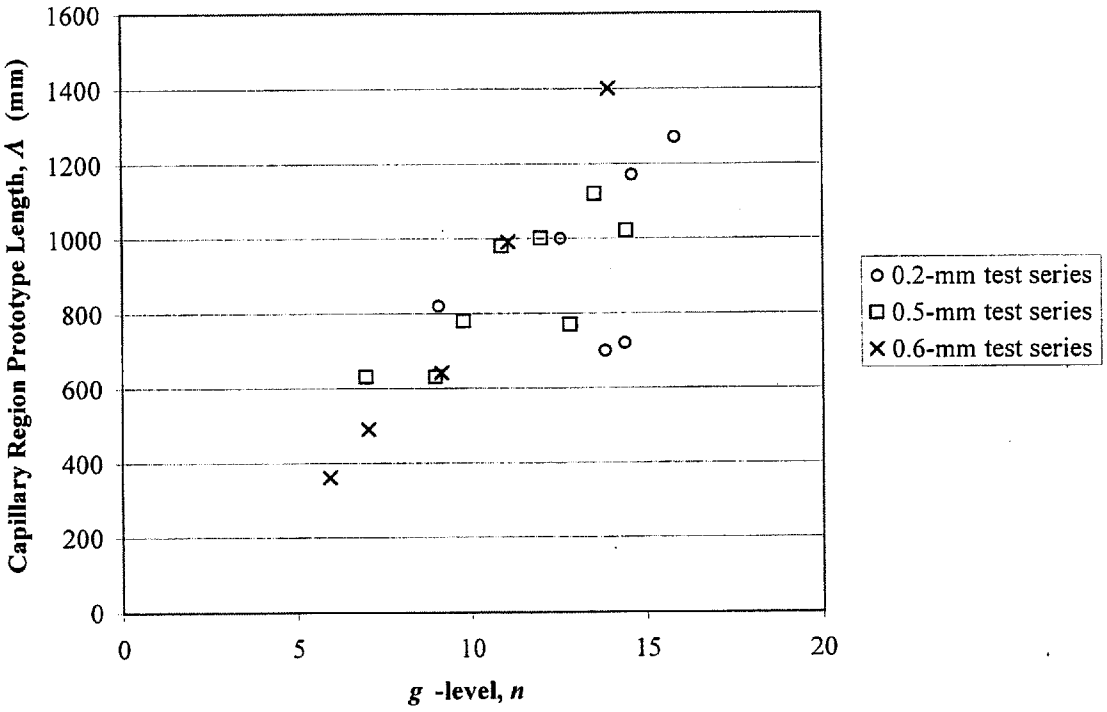

Figure 4.5 Length of the capillary region in the prototype versus g-level.

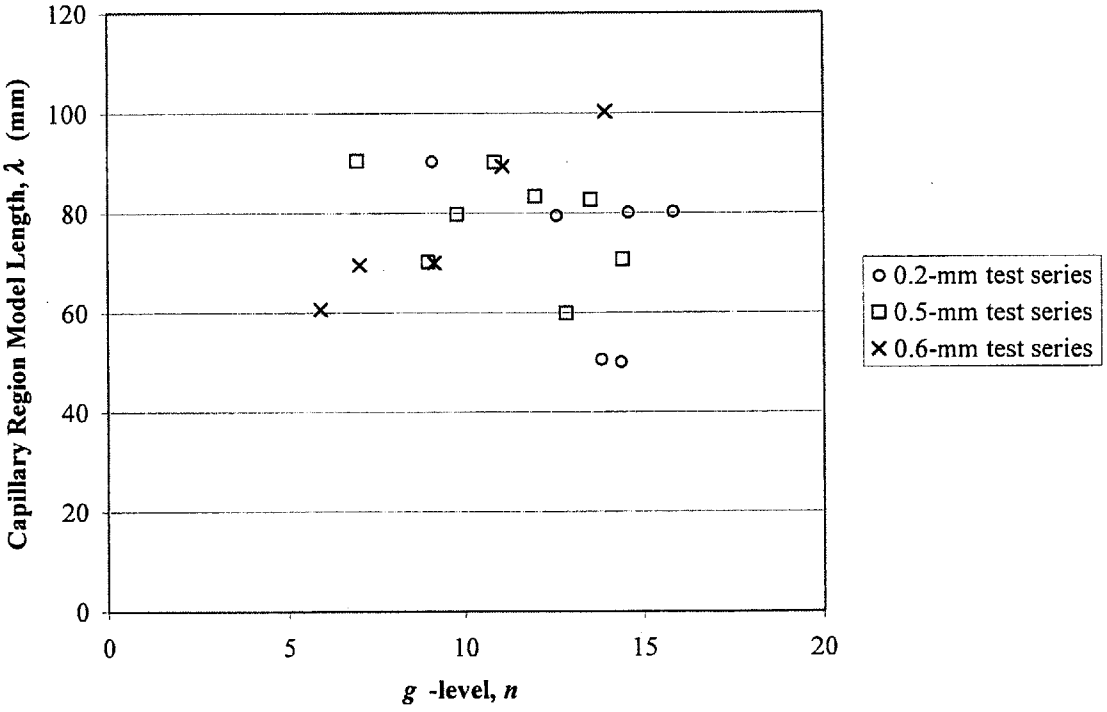

Figure 4.6 Length of the capillary region in the model versus g-level.

Chapter 5: DNAPL Flushing Test Results and Data

The test conditions and results for the DNAPL flushing tests performed in the laboratory are summarized in Table 5.1, below. The values of predicted Δz_C included in the table were calculated using Equation (2.17) and assume an average value of $\sigma \cos \theta$ = 0.032 N/m. Tests Lab 1 – Lab 4 were performed with the system closed to the graduated cylinder, so no z-levels were recorded.

5.1 Mobilization Pressure Data

The measured and predicted values of Δz_C are compared in Figure 5.1 for the 1.33-mm test series and in Figure 5.2 for the 2.70-mm test series. The theoretical curves for these figures again use an average value of the measured interfacial tension, $\sigma \cos \theta$.

In several of the 1.33-mm tests, the DNAPL plug was placed in the capillary tube so that the top of the plug was flush with the top of the tube. These tests are noted on Table 5.1 and identified with circular markers on Figure 5.1. In the remainder of the 1.33-mm tests and all of the 2.70-mm tests, the plug was placed 14-172 mm below the top of the capillary tube.

5.2 Interface Displacement

For selected tests, the displacement of the DNAPL-water interface with time was also recorded. Figure 5.3 shows the displacement profile obtained for Lab 8b, which had a plug length, h, of 454 mm, while Figure 5.4 shows the profile for Lab 9, which had a plug length of 159 mm. In both tests, the DNAPL plug was initially submerged in the tube.

For several tests, the applied gradient, Δz, was also recorded over time. Figure 5.5 plots changes in both x and Δz with time, t, for Lab 13. Point A, at approximately 410 seconds, is the time when the plug began to displace in the capillary tube. Point B, at approximately 810 seconds, is the time of maximum Δz during the test. Point C, at 899

seconds, is the time when the bottom of the DNAPL plug exited the capillary tube. For these graphs only, time zero corresponds to the beginning of the test and not the onset of plug motion.

As described in Section 3.4.3, several experiments were performed where the system was not open to the graduated cylinder. The displacement profiles obtained for some of these tests (Lab 1 - Lab 4 in Table 5.1) are plotted on Figure 5.6. For comparison, the velocity predicted by the flowrate alone (i.e., the displacement expected for a tube filled with water) is also plotted.

5.3 Data Interpretation

Figure 5.1 indicates reasonable agreement between measured and predicted values of Δz_C. The predictions are better for submerged tests than tests where the plug began at the top of the tube. This could be due to a difference in the shape of the DNAPL-water interface at the top of the plug for the submerged and non-submerged cases. Figure 5.7 depicts the possible shape of the interface for both cases; note that these figures are exaggerated to show detail. In the non-submerged case, due to conditions at the top of the capillary tube, a greater area of DNAPL at the top of the plug may be exposed to water. This would effectively increase the diameter of the plug relative to the submerged case. An increased d would yield a decrease in Δz_C, which is consistent with the data plotted on Figure 5.1.

All data plotted on Figure 5.2 are from submerged tests. There is reasonable agreement between the measured and predicted values of Δz_C for this series, as well.

The interface displacement data reported in Figure 5.3, Figure 5.4, and Figure 5.5(a) exhibit the same trend: initial plug velocity is very slow; the velocity increases gradually for a time, then increases rapidly until the plug exits the tube. This trend can be explained by examining the variation in gradient with time, as reported on Figure 5.5(b). The figure shows that Δz increases at an approximately constant rate until it reaches Δz_C (point A on the Figure), at which time plug motion begins. Plug motion is initially slow

as Δz continues to increase. However, at point B on the figure, pressure in the system reaches another critical value. The gradient, Δz, reaches its maximum and the plug accelerates rapidly, almost exponentially, to the tube exit (point C). During this interval (B to C), Δz decreases rapidly as the pressure buildup in the system is released.

One phenomenon observed in the submerged tests was the interruption of flow when the top of the DNAPL plug reached the top of the capillary tube. In the experiment depicted by Figure 5.4, the plug initially displaced slowly and then gradually increased in velocity, as described above. Plug velocity appeared to be reaching an interval of rapid acceleration. However, when the plug reached the top of the tube (shown as a dashed line on Figure 5.4), upward motion stopped for a few seconds. When displacement resumed, it was again at a slow rate and velocity began to gradually increase. After a certain time (approximately 240 seconds, in this case), the plug did achieve rapid acceleration and exited the tube.

This phenomenon is not as notable on Figure 5.3, which also depicts a submerged test. This could be due to the longer plug length, which would increase the momentum of the plug and make halting or slowing displacement more difficult once the plug is in motion. Alternatively, this difference could be because the plug on Figure 5.3 was submerged lower in the tube than the plug on Figure 5.4. This means that it had been in motion longer and achieved a higher velocity (approximately 3 mm/s as compared to 0.4 mm/s for the shorter test) by the time it reached the top of the tube. This would also increase momentum and decrease the potential impact of end effects.

The displacement profiles presented in Figure 5.6 illustrate that the system is indeed demonstrating plug flow behavior, as assumed in Section 2.1.3. The displacement of each plug is at a constant rate that is approximately equal to the injection flowrate of the flushing water. This confirms that there is little, or no, water channeling along or through the DNAPL and that the DNAPL is, in fact, displacing as a plug. This is consistent with visual observations of the displacement during the test.

Table 5.1 Summary of Flushing Experiments Performed

Test No.	d (mm)	l (mm)	Position of plug in tube	h (mm)	Measured Δz_c (mm)	Predicted Δz_c (mm)
Lab 1	2.70	1210	at top	198	–	–
Lab 2	2.70	1210	at top	208	–	–
Lab 3	2.70	1210	at top	285	–	–
Lab 4	2.70	1210	at top	489	–	–
Lab 8a	1.33	1210	submerged	80	7.4	15.6
Lab 8b	1.33	1210	submerged	454	38.6	42.6
Lab 9	1.33	1210	submerged	159	15.2	21.3
Lab 10	1.33	1210	at top	116	9.5	18.2
Lab 11	1.33	1210	at top	451	28.0	42.4
Lab 12	1.33	1210	submerged	776	55.5	65.8
Lab 13	1.33	1210	submerged	852	64.2	71.3
Lab 14	1.33	1210	at top	891	60.6	74.1
Lab 15	2.70	1210	submerged	111	8.8	12.9
Lab 16	2.70	1210	submerged	294	24.4	26.1
Lab 17	2.70	1210	submerged	557	40.0	45.0
Lab 18	2.70	1210	submerged	902	61.3	69.9
Lab 19	2.70	1210	submerged	1149	78.4	87.7

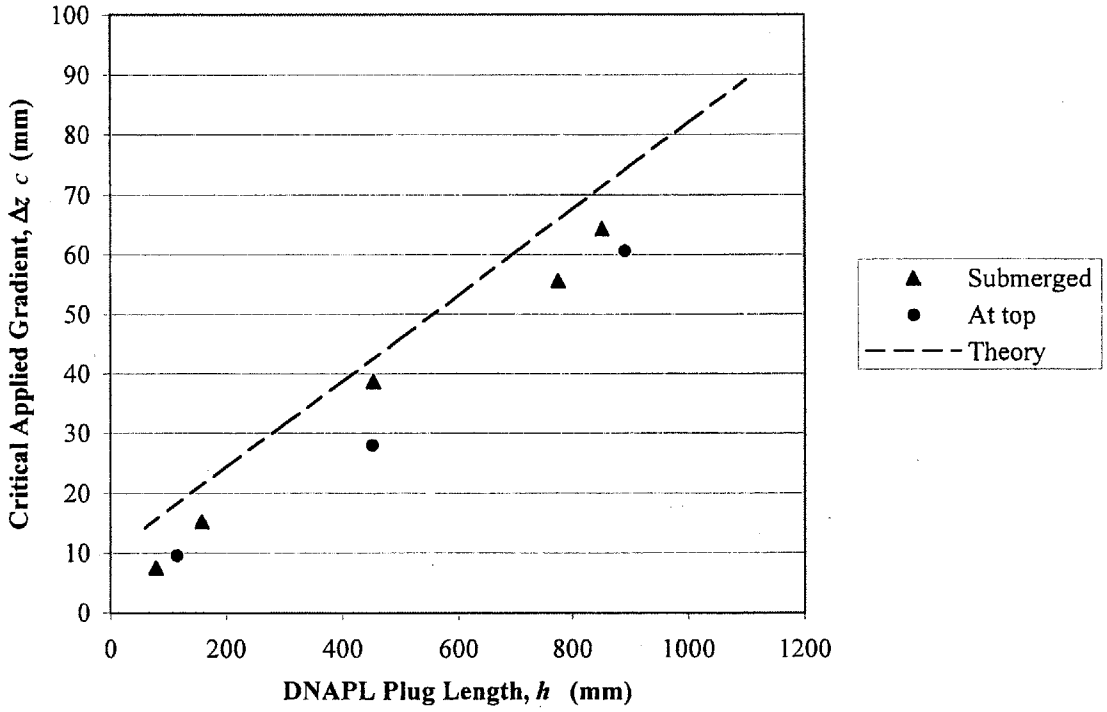

Figure 5.1 Critical applied gradients for 1.33-mm capillary tube series.

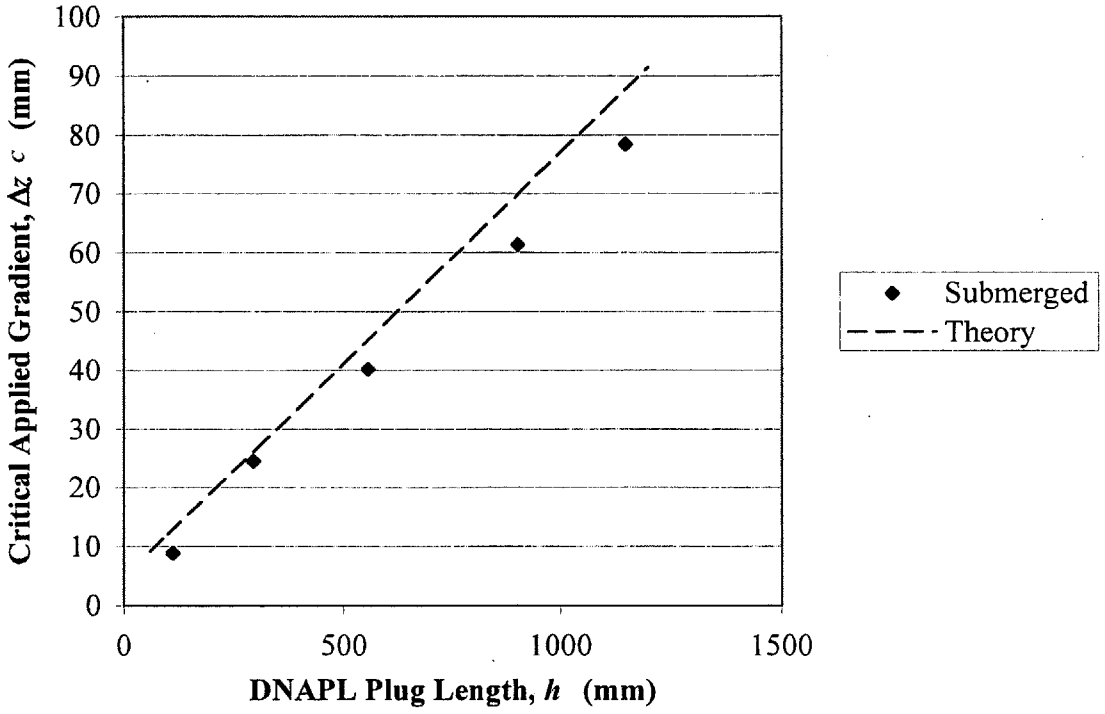

Figure 5.2 Critical applied gradients for 2.70-mm capillary tube series.

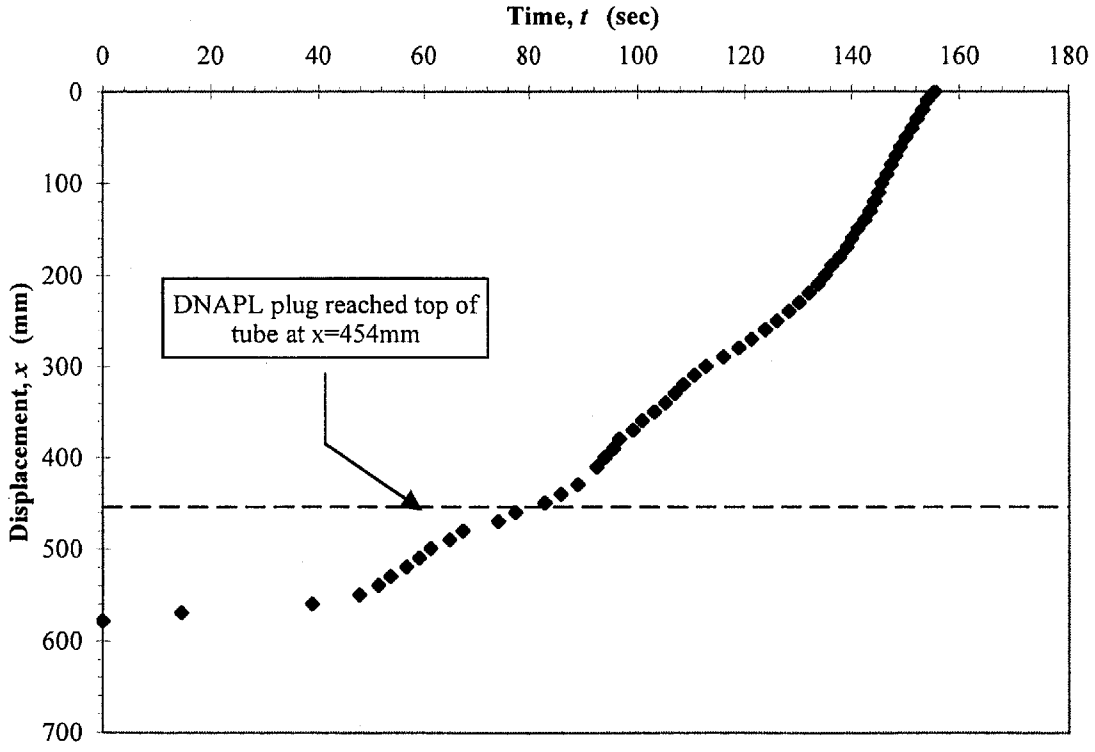

Figure 5.3 Displacement of DNAPL-water interface for Test Lab 8b, h = 454 mm.

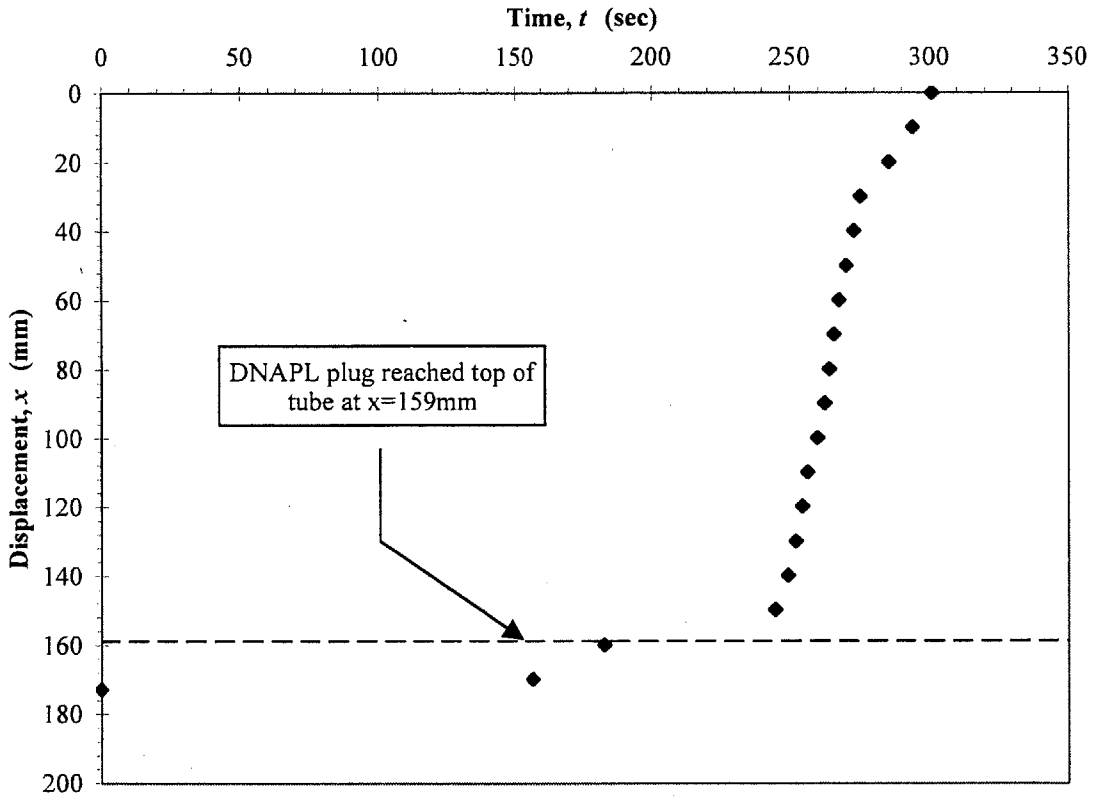

Figure 5.4 Displacement of DNAPL-water interface for Test Lab 9, h = 159 mm.

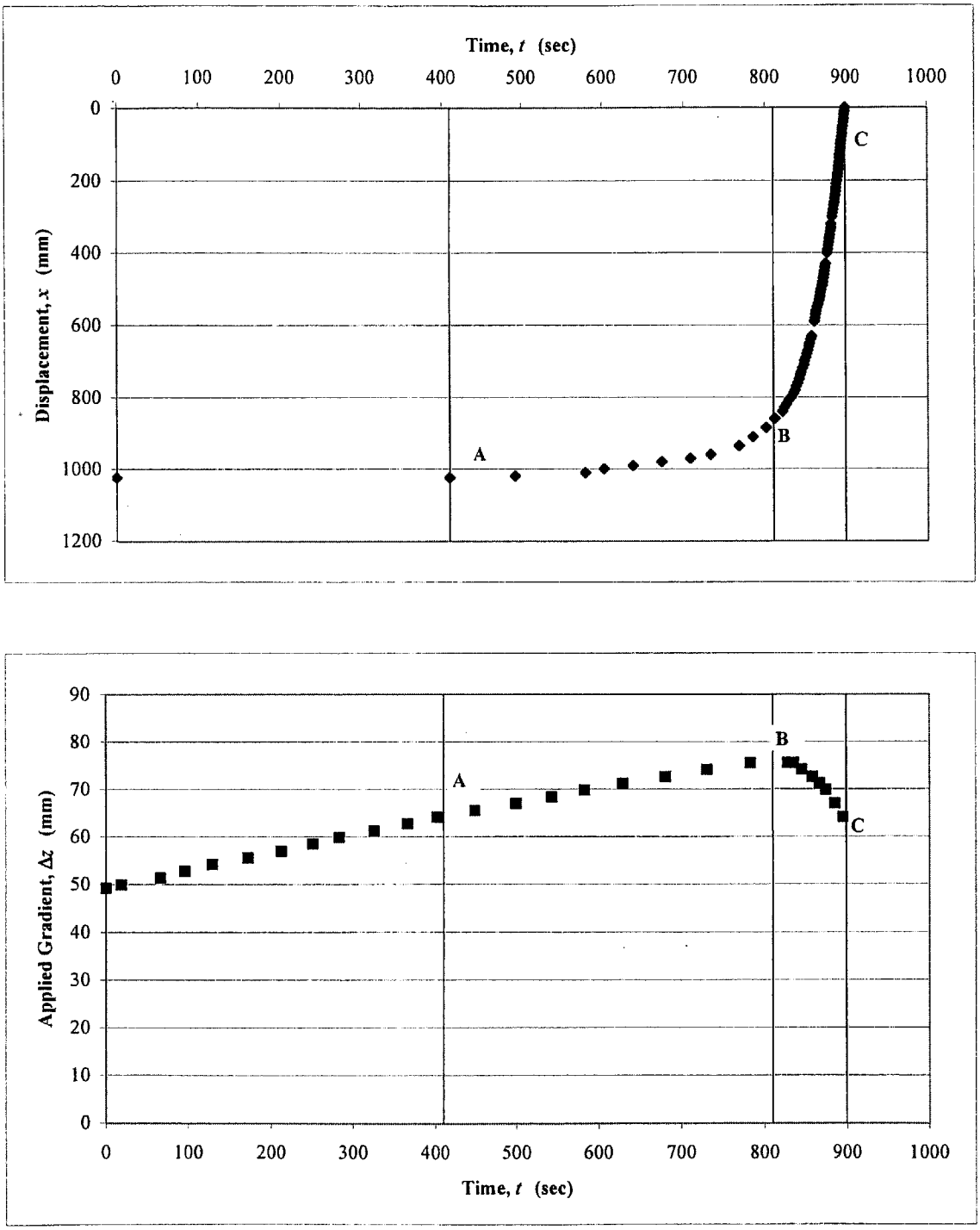

Figure 5.5 (a) Displacement of DNAPL-water interface for Test Lab 13.
(b) Applied gradient versus time for Test Lab 13.

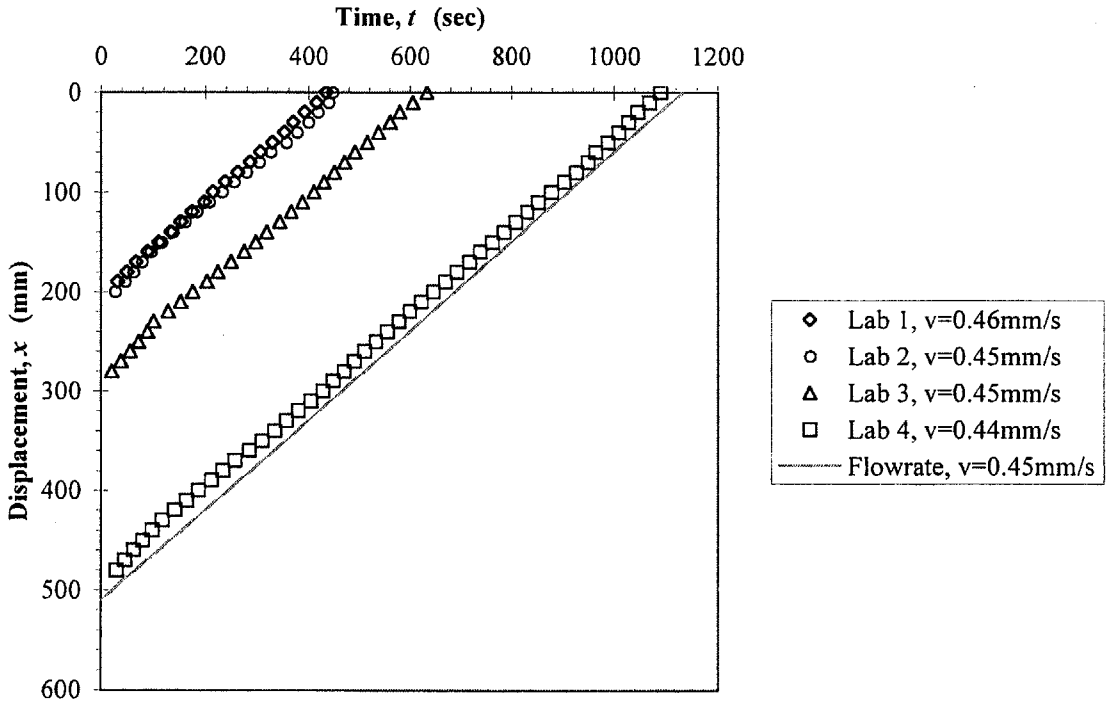

Figure 5.6 Displacement profiles for constant flow tests.

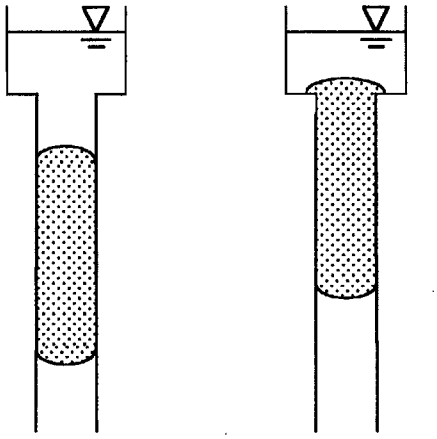

Figure 5.7 Possible difference in meniscus shape for submerged and non-submerged cases.

Chapter 6: Conclusions and Recommendations

6.1 Conclusions

6.1.1 DNAPL Invasion Tests

This thesis examined the invasion behavior of DNAPL in water-saturated, smooth-walled, planar-shaped, vertical fractures. For ease of study, the fractures were idealized as vertical capillary tubes of rectangular cross-section, and experiments were performed at a reduced scale using a geotechnical centrifuge.

A series of centrifuge experiments for fractures of various apertures demonstrated that a simple static model (Equation (2.23)) reasonably predicts the prototype DNAPL pool height that can be developed before invasion occurs. In addition, for centrifuge tests where the parameter α is small compared to 1, a dynamic model derived from the Navier-Stokes equations (Equation (2.25)) reasonably predicts the asymptotic displacement behavior of the DNAPL-water interface and its exit velocity.

There is some disagreement between the theoretical model and the experimental results at early stages of invasion; for all tests, the experiments showed a slower interface velocity than that predicted by the model. This phenomenon was attributed to the existence of a non-scalable "capillary region", where variations in the contact angle at early stages of invasion affect the interface velocity. For full-scale, field conditions, the capillary region would not likely extend beyond the first few centimeters of a fracture typically meters long. Therefore, this phenomenon is likely negligible in real fractures.

All results obtained were consistent with those obtained by Levy et al. [submitted for publication-b] for idealized fractures of circular cross-section.

6.1.2 DNAPL Flushing Tests

This thesis also examined the behavior of DNAPL plugs in water-saturated, smooth-walled, circular-shaped, vertical fractures under upward displacement conditions. For

these experiments, the fractures were idealized as vertical capillary tubes of circular cross-section at full-scale, and were tested at 1-*g* in the laboratory.

A series of laboratory experiments for fractures of 1.33-mm and 2.70-mm apertures demonstrated that a theoretical model based on a pressure balance (Equation (2.17)) reasonably predicts the pressure gradient that must be created in the system to mobilize a DNAPL plug trapped in the fracture. For all tests, the measured critical gradient was less than the predicted gradient; hence, the model is conservative.

Some initial observations were also made concerning the dynamic behavior of the DNAPL plug as it displaced upward in the idealized fracture. At early stages of displacement, the velocity of the DNAPL-water interface was slow. However, it gradually increased until the applied gradient reached a maximum value, after which the interface velocity increased rapidly until the plug exited the fracture. For tests in which the DNAPL plug was initially submerged in the fracture, there was an observable interruption of the flow pattern when the plug reached the top of the fracture. This phenomenon was less pronounced for plugs of greater momentum, due to longer plug length or greater velocity before reaching the top of the fracture.

Experimental results confirmed that there was little, or no, water channeling along or through the DNAPL in the fracture, and that the DNAPL displaced as a plug in the smooth-walled fractures.

The results obtained in these experiments suggest that hydraulic flushing might be developed into a feasible remediation technique for removing residual DNAPL from fractured rock or clay if the fracture roughness does not dominate the flow dynamics.

6.2 Recommendations

6.2.1 DNAPL Invasion Tests

The following additions to this experimental program are recommended:

- Study of the invasion behavior of DNAPL in rough-walled vertical fractures in order to determine how the resulting changes in aperture and contact angle would affect displacement.
- Observation of DNAPL invasion in glass or plastic reproductions of real, rough-walled fractures.
- Modeling and testing of the behavior of DNAPL in inclined fractures. Frictional forces could become more important and it is possible that there would be some water channeling on top of the DNAPL finger, i.e., the DNAPL might not displace as a plug.

6.2.2 DNAPL Flushing Tests

Further development of this experimental program could include:

- More precise measurement of the critical gradient, Δz_C, required to mobilize a trapped DNAPL plug. The precision of this experiment could be improved by eliminating the constant flowrate pump and connecting the graduated cylinder and capillary tube to form a closed system (identical to a u-tube manometer). Water could be added incrementally to the graduated cylinder until the plug displaced. This would eliminate the need to discern between changes in the shape of the DNAPL-water interface and actual displacement of the interface.
- Development of a theoretical model to describe the dynamic displacement behavior of a DNAPL plug under upward-flow conditions. Observations made during experiments performed for this thesis suggest that, as the plug displaces in the fracture, a DNAPL pool forms on top. Therefore, the model development process might be iterative. However, as a first approximation, the pool shape could be

modeled as a sphere (when the radius of the pool is less than the radius of the reservoir tube) or a cylinder (when the radius of the pool is equal to the radius of the reservoir tube).

- Observation of plug displacement with a DNAPL pool already in place on top of the fracture. This setup represents a common field condition.
- Observation of the system while maintaining a constant applied gradient, Δz. This would simulate a field remediation condition where, using the critical gradient value predicted by Equation (2.17) or some higher value of Δz, a constant gradient would be applied to flush DNAPL from the fracture system. The interface displacement behavior would be expected to be different than that discussed in this thesis, where Δz both increased and decreased during the time the plug displaced.
- Addition of surfactants or other additives to the flushing water to examine how changes in the interfacial tension, density contrast, or viscosity contrast would affect both the critical gradient required and the subsequent plug displacement behavior.
- Extension of these tests to fractures of planar shape and rough-walled fractures to better simulate real fractures.

References

Bear, J. (1972). *Dynamics of Fluids in Porous Media*, American Elsevier Pub. Co., New York.

Budavari, S. (1996). "The Merck Index: An Encyclopedia of Chemicals, Drugs, and Biologicals." , Merck, Whitehouse Station, N. J.

Chown, J. C., Kueper, B. H., and McWhorter, D. B. (1997). "The use of upward hydraulic gradients to arrest downward DNAPL migration in rock fractures." *Ground Water*, 35(3), 483-491.

Culligan, P. J., and Barry, D. A. (1998). "Similitude requirements for modelling NAPL movement with a geotechnical centrifuge." *Proceedings of the Institution of Civil Engineers Geotechnical Engineering*, 131(3), 180-186.

Culligan-Hensley, P. J., and Savvidou, C. (1995). "Environmental geomechanics and transport processes." Geotechnical Centrifuge Technology, R. N. Taylor, ed., Blackie Academic & Professional, London, 196-263.

Foster, D., Priore, S., and Brewer, K. "Behavior of DNAPLs in fractured bedrock." *Proceedings of the 1996 Specialty Conference*, Washington, DC, USA, 583-594.

Howard, P. H., and Meylan, W. M. (1997). "Handbook of Physical Properties of Organic Chemicals." , Lewis Publishers, Boca Raton, Fla.

Kueper, B. H., Haase, C. S., and King, H. L. (1992). "Leakage of dense, nonaqueous phase liquids from waste impoundments constructed in fractured rock and clay: Theory and case history." *Canadian Geotechnical Journal*, 29(2), 234-244.

Kueper, B. H., and McWhorter, D. B. (1991). "The behavior of dense, nonaqueous phase liquids in fractured clay and rock." *Ground Water*, 29(5), 716-728.

Levy, L. C., Culligan, P. J., and Germaine, J. T. (1998). "Investigation into DNAPL transport in fractures using capillary tubes." Centrifuge 98, T. Kimura, O. Kusakabe, and J. Takemura, eds., Balkema, Rotterdam, 607-612.

Levy, L. C., Culligan, P. J., and Germaine, J. T. (submitted for publication-a). "DNAPL transport in smooth-walled, vertical fractures: Part I - Theoretical model and laboratory experiments." *Water Resources Research.*

Levy, L. C., Culligan, P. J., and Germaine, J. T. (submitted for publication-b). "DNAPL transport in smooth-walled, vertical fractures: Part II - Physical modeling using the geotechnical centrifuge." *Water Resources Research.*

Lide, D. R. (1993). *CRC Handbook of Chemistry and Physics*, CRC Press, Boca Raton, Florida.

Longino, B. L., and Kueper, B. H. (1995). "The use of upward gradients to arrest downward dense, nonaqueous phase liquid (DNAPL) migration in the presence of solubilizing surfactants." *Canadian Geotechnical Journal*, 32(2), 296-308.

Longino, B. L., and Kueper, B. H. (1996). "Retention of dense nonaqueous phase liquid (DNAPL) in fractured rock." Proceedings of the 2nd North American Rock Mechanics Symposium: NARMS'96. A Regional Conference of ISRM/Montreal/Quebec/Canada/19-21 June 1996. Rock Mechanics Tools and Techniques, M. Auberti, F. Hassani, and H. Mitri, eds., Balkema, Rotterdam, 1353-1358.

Longino, B. L., and Kueper, B. H. (1999). "Nonwetting phase retention and mobilization in rock fractures." *Water Resources Research*, 35(7), 2085-2093.

National Research Council. (1994). *Alternatives for Ground Water Cleanup*, National Academy Press, Washington, D. C.

Pankow, J. F., Feenstra, S., Cherry, J. A., and Ryan, M. C. (1996). "Dense chlorinated solvents in groundwater: Background and history of the problem." Dense Chlorinated Solvents and Other DNAPLs in Groundwater: History, Behavior, and Remediation, J. F. Pankow and J. A. Cherry, eds., Waterloo Press, Portland, Oreg., 1-52.

Parker, B. L., McWhorter, D. B., and Cherry, J. A. (1997). "Diffusive loss of non-aqueous phase organic solvents from idealized fracture networks in geologic media." *Ground Water*, 35(6), 1077-1088.

Ratnam, S. (1996). "Geotechnical centrifuge modeling of the behavior of light nonaqueous phase liquids (LNAPLs) in sand samples under hydraulic flushing," M.S., Massachusetts Institute of Technology.

Reitsma, S., and Kueper, B. H. (1994). "Laboratory measurement of capillary pressure-saturation relationships in a rock fracture." *Water Resources Research*, 30(4), 865-878.

Schofield, A. N. (1980). "Cambridge geotechnical centrifuge operations." *Géotechnique*, 30(3), 227-268.

Slough, K. J., Sudicky, E. A., and Forsyth, P. A. (1999). "Importance of rock matrix entry pressure on DNAPL migration in fractured geologic materials." *Ground Water*, 37(2), 237-244.

Stephens, D. B., Kelsey, J. A., Prieskat, M. A., Piepho, M. G., Shan, C., and Ankeny, M. D. (1998). "DNAPL migration through a fractured perching layer." *Ground Water*, 36(4), 605-610.

Yaws, C. L. (1995). *Handbook of Viscosity*, Gulf Pub. Co., Houston.